

The SDSS-II Supernova Survey: Parameterizing the Type Ia Supernova Rate as a Function of Host Galaxy Properties

Mathew Smith^{1,2,3}, Robert C Nichol², Benjamin Dilday^{4,5}, John Marriner⁶,
 Richard Kessler^{7,8}, Bruce Bassett^{3,9,10}, David Cinabro¹¹, Joshua Frieman^{6,7,8},
 Peter Garnavich¹², Saurabh W Jha¹³, Hubert Lampeitl², Masao Sako¹⁴,
 Donald P Schneider¹⁵, Jesper Sollerman¹⁶

mathew.smith@uct.ac.za

ABSTRACT

Using data from the Sloan Digital Sky Supernova Survey-II (SDSS-II SN Survey), we measure the rate of Type Ia Supernovae (SNe Ia) as a function of galaxy properties at intermediate redshift. A sample of 342 SNe Ia with $0.05 < z < 0.25$ is constructed. Using broad-band photometry and redshifts we use the PÉGASE.2 spectral energy distributions (SEDs) to estimate host galaxy stellar masses and recent star-formation rates. We find that the rate of SNe Ia per unit stellar mass is significantly higher (by a factor of ~ 30) in highly star-forming galaxies compared to passive galaxies. When parameterizing the SN Ia rate (SNR_{Ia}) based on host galaxy properties, we find that the rate of SNe Ia in passive galaxies is not linearly proportional to the stellar mass, instead a $\text{SNR}_{\text{Ia}} \propto M^{0.68}$ is favored. However, such a parameterization does not describe the observed SN Ia rate in star-forming galaxies. The SN Ia rate in star-forming galaxies is well fit by $\text{SNR}_{\text{Ia}} = 1.05 \pm 0.16 \times 10^{-10} M^{0.68 \pm 0.01} + 1.01 \pm 0.09 \times 10^{-3} \dot{M}^{1.00 \pm 0.05}$ (statistical errors only), where M is the host galaxy mass (in M_{\odot}) and \dot{M} is the star-formation rate (in $M_{\odot} \text{ yr}^{-1}$). These results are insensitive to the selection criteria used, redshift limit considered and the inclusion of non-spectroscopically confirmed SNe Ia. We also show there is a dependence between the distribution of the MLCS light-curve decline rate parameter, Δ , and host galaxy type. Passive galaxies host less luminous SNe Ia than seen in moderately and highly star-forming galaxies, although a population of luminous SNe is observed in passive galaxies, contradicting previous assertions that these SNe Ia are only observed in younger stellar systems. The MLCS extinction parameter, A_V , is similar in passive and moderately star-forming galaxies, but we find indications that it is smaller, on average, in highly star-forming galaxies. We confirm this result using the SALT2 light-curve fitter.

Subject headings: Cosmology:observations — distance scale — Galaxies:evolution — supernovae:general

¹Astrophysics, Cosmology and Gravity Centre (ACGC), Department of Mathematics and Applied Mathematics, University of Cape Town, Rondebosch, 7701, SA

²Institute of Cosmology and Gravitation, University of Portsmouth, Portsmouth, PO1 3FX, UK

³African Institute for Mathematical Sciences, 6-8 Melrose Road, Muizenberg 7945, SA

⁴Las Cumbres Observatory Global Telescope Network, 6740 Cortona Dr., Suite 102, Goleta, CA 93117, USA

⁵Department of Physics, University of California, Santa Barbara, Broida Hall, Mail Code 9530, Santa Barbara, CA

93106-9530, USA

⁶Center for Particle Astrophysics, Fermilab, P.O. Box 500, Batavia, IL 60510, USA

⁷Department of Astronomy & Astrophysics, The University of Chicago, 5640 S. Ellis Ave, Chicago, IL 60637, USA

⁸Kavli Institute for Cosmological Physics, The University of Chicago, 5640 S. Ellis Ave, Chicago, IL 60637, USA

⁹South African Astronomical Observatory, P.O. Box 9, Observatory 7935, South Africa

¹⁰Department of Mathematics and Applied Mathemat-

1. Introduction

Type Ia supernovae (SNe Ia) have been extensively studied because they provide accurate relative distances on cosmological scales. Measurements of SNe Ia have indicated that the expansion of the universe is currently accelerating (Riess et al. 1998; Astier et al. 2006; Wood-Vasey et al. 2007; Kessler et al. 2009a; Lampeitl et al. 2010a), leading to the introduction of a “Dark Energy” component in our model of the Universe.

SNe Ia are thought to arise from carbon-oxygen white dwarfs that accrete mass from a companion star and approach the Chandrasekhar mass limit, resulting in a thermonuclear explosion (Hoyle & Fowler 1960; Branch et al. 1995; Yungelson & Livio 1998). However, there is still significant debate on the details; e.g. the explosion mechanism, the accretion process, and the progenitor companion star, which may be a giant star, a main sequence star, or a secondary white dwarf (Höflich et al. 2003). A measurement of the delay time (*i.e.*, the time between the formation of the binary system and its thermonuclear explosion), constrains the possible progenitor systems (Greggio 2005). The delay time distribution can be determined observationally by comparing the observed SNe Ia rates in galaxies with different star-formation histories (Gal-Yam & Maoz 2004).

It has been observationally determined that SNe Ia are distinctly more common in galaxy hosts with recent star-formation activity (Oemler & Tinsley 1979). Recent work has determined that the SNe Ia rate per unit stellar mass depends on host galaxy morphology and (B-K) color

(Mannucci et al. 2005) and that the SN Ia rate in late-type galaxies is a factor ~ 20 higher than in E/S0 galaxies. SNe Ia are seen locally to be rarer in galaxy bulges than spiral arms (Wang et al. 1997) and more common in blue galaxies than red (Mannucci et al. 2005). The population associated with star-formation suggests that the SN Ia rate contains a population with a cosmologically short time delay, while the observation of SNe Ia in very old systems indicates the existence of a population with large time delay (Cappellaro et al. 1999).

Scannapieco & Bildsten (2005) and later Mannucci et al. (2006) and Sullivan et al. (2006) proposed a “two-component” SN Ia rate, consisting of a prompt component, dependent on recent host galaxy star-formation, and a delayed component dependent on galaxy stellar mass. The overall SN Ia rate is thus the sum of these two components, and can be further generalised as a function of the galaxy star-formation rate and stellar mass. Observations strongly favor a two-component model over a single component model (Sullivan et al. 2006) and since the cosmic star-formation rate increases with redshift, we expect that the prompt component will become a larger fraction of the SN Ia population with increasing redshift. Maoz et al. (2010), using cluster rate measurements, suggest a universal delay time distribution, independent of environment and parameterized by $\text{SNR}_{\text{Ia}} \propto t^{-1.2 \pm 0.3}$.

Several attempts have been made to constrain the functional form of the SNe Ia rate. Sullivan et al. (2006), using 124 SNe Ia from the SNLS survey, found that, for passive galaxies, the SNe Ia rate is consistent with a linear relationship with host galaxy stellar mass. Recently, Li et al. (2010), used a sample of 274 SNe Ia from the LOSS survey, to consider how the size and morphology of the host galaxy affects the SNe Ia rate. They favor a power-law relationship between galaxy stellar mass and the SNe Ia rate (SNuM) with exponent approximately one half independent of both galaxy morphology and color. Maoz et al. (2010) find evidence for both a “prompt” (age < 420 Myr) and “delayed” component ranging between 2.4 and 13 Gyr. Li et al. (2010) also show that SN Ia rate in young stellar populations may be strongly correlated with the rate of core-collapse SN.

A SN Ia rate composed of two components may have ramifications when SNe Ia are used to de-

ics, University of Cape Town, Rondebosch, 7701, SA

¹¹Wayne State University, Department of Physics and Astronomy, Detroit, MI, 48201, USA

¹²Department of Physics, University of Notre Dame, 225 Nieuwland Science Hall, Notre Dame, IN 46556, USA

¹³Department of Physics and Astronomy, Rutgers, the State University of New Jersey, 136 Frelinghuysen Road, Piscataway, NJ 08854, USA

¹⁴Physics & Astronomy, University of Pennsylvania, 209 South 33rd Street, Philadelphia, PA 19104

¹⁵Department of Astronomy and Astrophysics, Pennsylvania State University, 525 Davey Laboratory, University Park, PA 16802, USA

¹⁶The Oskar Klein Centre, Department of Astronomy, AlbaNova, Stockholm University, SE-106 91 Stockholm, Sweden

termine cosmological parameters. Since the two components are likely to have two different progenitor systems, the common assumption that all SNe Ia can be normalized in the same way is in question. It is likely that two distinct progenitor systems would contribute to the observed intrinsic scatter in the distances measured with SNe Ia. The relation between light-curve decline rate and peak luminosity for SNe Ia has been well tested (Phillips 1993; Howell et al. 2007), but the physics behind this relation and the details of the explosion mechanism are only partially understood (Kasen & Woosley 2007). Better understanding of the nature of SNe Ia explosions and progenitor systems will aid in improving the accuracy of SN Ia distance measurements (Lampeitl et al. 2010b; Sullivan et al. 2010).

The total SN Ia rate has been well studied. Neill et al. (2006) and Graur et al. (2011) have constrained on the SN Ia rate at high redshift, using the SNLS dataset to $z = 0.5$ and SNe Ia from the Subaru Deep Field (SDF) to $z < 2$, respectively. Dilday et al. (2008) determined the most accurate SNe Ia rate at intermediate redshift using the first year SDSS-II SN dataset to $z \leq 0.12$ and extended the analysis to $z < 0.3$ in Dilday et al. (2010).

In this paper, we investigate the characteristics of the host galaxies of SNe Ia at intermediate redshift using the SDSS-II SN dataset following the methodology described in Sullivan et al. (2006). The SDSS-II SN survey is ideally suited to this task because it provides the largest, unbiased dataset currently available, with well understood efficiency corrections, in a redshift range fully in the Hubble flow, but with high signal-to-noise observations. Our host galaxies are well measured in several filter bands, allowing us to accurately estimate the galaxy’s properties. The aim of this work is to measure the rate of SNe Ia explosions as a function of the host galaxy stellar mass and star-formation rate. We parameterize the relationship for our intermediate redshift data, and interpret the results in the context of the two-component model.

This paper is organized as follows. In §2 we describe the SDSS-II SN Survey, the observing strategy and give a brief account of the results of this survey. In §3 we show how the SDSS-II SN dataset is incomplete and introduce a method to produce

an unbiased sample with a well understood efficiency correction. In §4 we outline how the host galaxy of each SNe Ia is identified and the method that we use to determine the derived properties of the host galaxy. We also describe the sample of field galaxies used for comparison, and how it is corrected for incompleteness. In §6 we investigate how the SN Ia rate is dependent on the properties of the host galaxy, studying how it is dependent on the stellar mass of the galaxy (§6.1), the star-formation rate of the host galaxy (§6.3), and the specific star-formation rate of the host (§6.5). Finally, §7 discusses how the light-curve shape (§7.1) and extinction (§7.2) of the SN Ia events are related to the galaxy host properties. Our conclusions are given in §8.

2. The SDSS-II SN Survey

In this work, we use the full sample from the SDSS-II SN Survey (Frieman et al. 2008). This provides one of the largest samples of SNe Ia currently available.

The SDSS-II SN Survey was a three year rolling search that produced a sample of spectroscopically confirmed SNe Ia with well-measured multi-color light-curves at intermediate redshift ($z < 0.4$) using the SDSS 2.5m telescope (York et al. 2000; Strauss et al. 2002; Gunn et al. 2006) at Apache Point Observatory with a wide field CCD camera (Gunn et al. 1998). Observations were made in the SDSS *ugriz* filters (Fukugita et al. 1996), alternating between the northern and southern “strips” of the field designated as “Stripe 82” (Stoughton et al. 2002), bounded by $-60^\circ < \alpha(\text{J2000}) < 60^\circ$, and $-1.258^\circ < \delta(\text{J2000}) < 1.258^\circ$. Adverse weather and bright moonlight resulted in an average observation of each strip once every four nights with typical limiting magnitudes of $g \sim 21.8$, $r \sim 21.5$, $i \sim 21.2$ per observation. The scene modelling photometry (SMP) technique of Holtzman et al. (2008) was used to produce accurate photometric data for each SN event.

The SDSS-II SN Survey identified many thousands of transient events, of which 513 were spectroscopically confirmed as SNe Ia and 85 were other SN types (Sako et al. 2008; Zheng et al. 2008). Spectroscopic redshifts for the host galaxies of 339 probable SNe Ia, based on their light-curves, were also obtained, and are discussed further in §3.

The first year SDSS-II SN sample was used for a cosmological analyses (Kessler et al. 2009a; Sollerman et al. 2009; Lampeitl et al. 2010a). Dilday et al. (2008, 2010) measured the SNe Ia volumetric rate, Lampeitl et al. (2010b); Gupta et al. (2011); Konishi et al. (2011) and D’Andrea et al. (2011) analyzed the effect of host galaxies on light-curve parameters, both from the photometric properties of the host galaxies and studying their spectral features.

The SDSS-II SN Survey is approximately magnitude limited, producing an otherwise unbiased sample. This analysis uses a sample of 342 SNe Ia in the redshift range $0.05 < z < 0.25$, where the efficiency of the survey is high (Dilday et al. 2010). This homogenous sample is comprised of 197 spectroscopically confirmed SNe Ia, with a further 87 having a host galaxy spectroscopic redshift. All objects are selected using a well defined selection criteria, and have well-measured light-curves that are consistent with a SNe Ia template, based on the Bayesian light-curve fitting method of Sako et al. (2008). The selection criteria used to create this sample is discussed in §3.

3. Incompleteness Corrections

There are two major sources of inefficiency in the SDSS-II SN pipeline that lead to potential biases in the spectroscopically confirmed SN sample: detection efficiency and spectroscopic incompleteness. The detection efficiency was primarily magnitude limited and is amenable to calculation by simulation. The spectroscopic selection and analysis depends on many factors that are difficult to quantify. We adopt a strategy of augmenting the sample of spectroscopically confirmed SNe Ia with a sample of photometrically classified SNe Ia, identified by their light-curve shape and color and correcting for detection efficiency.

3.1. Correcting for Spectroscopic Incompleteness

The SDSS-II SN Survey prioritized spectroscopic follow-up observations of SN candidates using a Bayesian classification method (Sako et al. 2008)¹. However, the final ranking and decisions on spectroscopic follow-up priorities were based on the telescope’s capabilities, local weather conditions and the SN position on the sky, thus leading

to a spectroscopic sample whose selection criteria are difficult to describe quantitatively. To produce a homogeneous sample of SN Ia candidates, we therefore seek a sample selection that avoids the uncertain and time-varying spectroscopic target selection process. We also seek a sample with high quality light-curves and low levels of contamination. However, we must also ensure that the majority of detected SNe Ia pass this criteria, so that our results are not dominated by the efficiency corrections.

We adopt a two-stage process. In the first stage, we use photometry obtained during the SN Ia search and the Bayesian classification method, to apply very loose cuts that are intended to reduce the large number of non-SN Ia transient objects that are classified as candidates by the SDSS-II search pipeline, while retaining any SN Ia that could possibly survive our subsequent quality cuts. This sample is then analyzed by the more accurate SMP photometry and fit by the MLCS2k2 light-curve fitter to obtain a sample of probable SN Ia. The criteria used for our two-stage process is described as follows.

Firstly, as part of the SDSS-II SN operations, every transient object with more than two epochs was selected to be a candidate, after known AGNs, variable stars and pipeline artifacts were removed. There are $\sim 20,000$ such candidates. The Bayesian classification technique, used in the SDSS-II SN search operations, fits SNe Ia, Ib/c and II template light-curves to each candidate, producing a probability, p_T , for a candidate to belong to each class (T) of SNe. This method assumes that each candidate is a SN of some particular type, but has been shown, nevertheless, to be accurate in differentiating between different SN types (Sako et al. 2008; Kessler et al. 2010). This Bayesian classification technique was applied to each candidate, and the following criteria was used to select viable SN Ia candidates:

- At least 3 search discovery epochs,
- $p_{Ia} > 0.45$,
- If the candidate has more than 5 search pho-

¹An updated version of this method is given in Sako et al. (2011). However, as our goal is to replicate the follow-up strategy of the SDSS-II SN Survey, it is not used in this work.

ometry epochs, the best-fit Ia model is not SN 2005gj².

Additional cuts were considered, including using the photometric redshift from the nearest host galaxy to constrain the light-curve, but were rejected, as it is significantly harder to model the SDSS-II SN survey selection function with those cuts. Our criteria select 1762 candidates, including 88% of the spectroscopically confirmed SNe Ia. Of the 12% of confirmed SNe Ia that fail this selection criteria, 27% (17) were only observed on one or two occasions, 70% (45) do not satisfy the p_{Ia} criteria, and 3% (2) are best-fit by a 2005gj-like template (including SN 2005gj itself).

The selection criteria described above, uses photometry obtained during the SN Ia search to produce a sample of candidates containing the vast majority of the spectroscopically confirmed SNe Ia, whilst removing the vast majority of non-SN Ia transient objects. In the second stage of our selection criteria, this sample was then analyzed using the more complete and more accurate SMP photometry and fit using the MLCS2k2 light-curve fitter (Jha et al. 2007; Kessler et al. 2009b) to ensure each candidate has a well covered light-curve and is well fit by an SN Ia event. The selection criteria are the same as were used by Kessler et al. (2009a) and Dilday et al. (2010), namely,

1. At least 5 photometric observations (all at different epochs) between -20 and $+60$ days relative to peak light in the rest-frame of the SN,
2. At least one epoch with signal-to-noise ratio > 5 in each of g , r , and i (not necessarily the same epoch in each passband),
3. At least one photometric observation at least 2 days prior to maximum brightness in the SN rest frame,
4. At least one photometric observation at least 10 days past maximum brightness in the SN rest frame,

²SN 2005gj (Aldering et al. 2006; Prieto et al. 2007) is a peculiar SN, with a flat light-curve after maximum. In addition to removing SN 2005gj-like SNe, this criterion also removes AGN and other non-transient events from our sample.

5. MLCS2k2 light-curve fit probability > 0.001 ³,
6. MLCS2k2 light-curve decline rate parameter of $\Delta > -0.4$ ⁴,
7. $-51^\circ < \alpha(\text{J2000}) < 57^\circ$.

Excess color in SNe Ia is interpreted by MLCS2k2 as extinction by dust in the host galaxy, parameterized using Cardelli et al. (1989), where $E(B - V) = A_V/R_V$. For this analysis, we adopt a value of $R_V = 2.3$ and assume an A_V prior in the fitting process of $P(A_V) = e^{-A_V/\tau}$, with $\tau = 0.33$, as described in Kessler et al. (2009a). For comparison, $R_V = 3.1$ on average for our galaxy, but previous SN Ia studies have favored values of $R_V \sim 2.0$ (Nobili & Goobar 2008; Lampeitl et al. 2010b).

Of the 1762 candidates that satisfy the Bayesian light-curve fitter criteria, 843 satisfy the sample selection. Of these 843, 319 are spectroscopically confirmed as SNe Ia and 180 are unconfirmed but have a host galaxy spectroscopic redshift.

The SNANA version (Kessler et al. 2009b) of MLCS is able to estimate a photometric redshift for SN candidates in addition to determining a distance modulus. Most of our 843 candidates lack spectroscopic redshift measurements, so we adopt a cosmological model of $\Omega_M = 0.3$ and $\Omega_\Lambda = 0.7$, to reduce the number of fit parameters, and to determine a photometric redshift for each candidate. To construct a sample that is unbiased with respect to spectroscopic follow-up, and has a well determined selection function, we fit for a photometric redshift for all candidates, regardless of whether a spectroscopic redshift is known. An analysis of the accuracy of these photometric redshift estimates is given in Dilday et al. (2010), who find that the photometric redshifts are negligibly biased and are accurate to ~ 0.01 at low redshift ($0 < z < 0.25$).

These selection criteria ensure that each candidate has a well covered light-curve that is well fit by a normal SN Ia event (peculiar SNe Ia will generally not pass the selection criteria).

³ 6 of the spectroscopically confirmed SNe Ia fail this criteria, including 4 peculiar SN Ia

⁴The cuts on MLCS2k2 light-curve fit probability and Δ (5,6) have a negligible effect on the size of our sample compared to the sampling cuts (1,2,3,4)

While we have relied on photometric redshifts for the initial sample selection, we use spectroscopic redshift information, when available, for redshift selection and all subsequent analysis. To construct a sample that is primarily comprised of spectroscopically confirmed SNe Ia and not dominated by photometrically classified SNe Ia, and to avoid low detection efficiency (see §3.2), we restrict our SN sample to the redshift range $0.05 < z < 0.25$. This leaves 379 SNe Ia. We find 217 (57%) are spectroscopically confirmed SNe Ia, while 94 (25%) are unconfirmed but have host galaxy spectroscopic redshifts and 68 (18%) have no spectroscopic redshift information. The number of candidates that satisfy each stage of our selection criteria is shown in Table 1. While the majority of our sample has been spectroscopically confirmed, a significant fraction of candidates are only photometrically classified. However, Dilday et al. (2010) conservatively estimated that there is a 3% probability for non-SNe Ia to satisfy our selection criteria, and the total estimated contamination by non-SNe Ia's is 2%.

Table 2 lists the number of SNe Ia that pass our selection criteria for several redshift ranges, including the proportion of each sample that is spectroscopically confirmed as SNe Ia. As expected, the proportion of spectroscopically confirmed SNe decrease with increasing redshift, but it remains above 50% out to $z = 0.25$.

3.2. Determining the Survey Efficiency

Having defined a homogeneous sample of SNe Ia candidates with $0.05 < z < 0.25$, we need to know the SDSS-II SN detection efficiency, $\epsilon(z)$. A detailed analysis of the efficiency was given in Dilday et al. (2008, 2010), differing here only in the use of MLCS fitted photometric redshifts to select the fake SNe that pass our redshift cut. Simulated SNe Ia, with a range of sky positions, time of peak brightness, redshifts, decline-rate parameters, extinction and host galaxy position, and realistic errors were added directly to the image data and were processed by the SDSS-II SN pipeline (Sako et al. 2008). The proportion of SNe Ia that satisfy the criteria defined in §3.1 is shown as a function of redshift in Figure 1 for each of the three years of the SDSS-II SN Survey. We also highlight the high redshift limit used in this analysis. Over 50% of SNe Ia are detected in our redshift range. The

fact that the efficiency is less than 100% at low redshift is caused by SN explosions that occur late or early in the observing season and fail to allow the required number of observations. This inefficiency is a major effect at all redshifts but is accurately modelled in our simulation. The uncertainty on the survey efficiency is discussed in detail in Dilday et al. (2010).

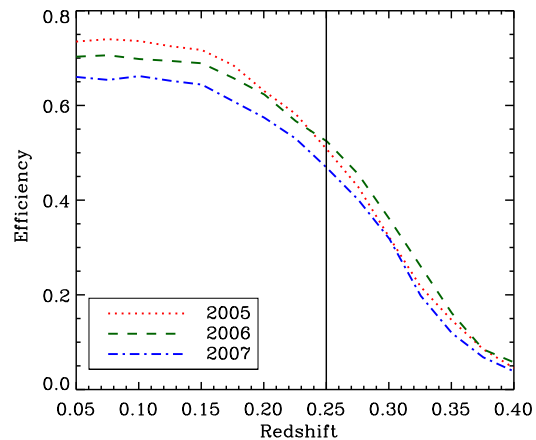


Fig. 1.— The efficiency of SN detection as a function of redshift for each observing season. The high redshift limit used in this analysis is also shown.

The survey efficiency considered for this analysis is a function of redshift. However, this functional form maybe too simplistic, as it assumes no variation in the intrinsic brightness of SNe Ia as a function of host galaxy type. To determine if our results are dependent on this assumption, we study how our conclusions are affected if parameterize the survey efficiency as a function of redshift, A_V and Δ . This additional correction produces results that are consistent with our nominal result, with differences of much less than 1σ . We thus consider the survey efficiency to be a function solely of redshift, but note that other analyses have not considered the effect of this assumption on their results.

We have now defined a uniformly selected sample of 379 SNe Ia candidates with $0.05 < z < 0.25$ from the three years of the SDSS-II SN Survey, and calculated the efficiency of the survey in this redshift range, which we shall invert to weight the galaxies in our sample. The uncertainty on

TABLE 1
NUMBER OF CANDIDATES PASSING EACH STAGE OF §3.1

	No. of Candidates	Spectroscopically confirmed
All SDSS-II SN candidates	19046	513
After Bayesian LC fit	1762	449
Passing Sample Selection	843	319
0.05 < z < 0.25	379	217

TABLE 2
NUMBER OF CANDIDATE SNe Ia AS A FUNCTION OF REDSHIFT

Redshift Limit	Total	Spectroscopically confirmed	Host Redshift	Photo-z only
0.05 < z < 0.10	21	19 (90.5%)	1 (4.8%)	1(4.8%)
0.05 < z < 0.15	88	73 (83.0%)	11 (12.5%)	4 (4.5%)
0.05 < z < 0.20	214	144 (67.3%)	47 (22.0%)	23 (10.7%)
0.05 < z < 0.25	379	217 (57.3%)	94 (24.8%)	68 (17.9%)
0.05 < z < 0.30	559	272 (48.7%)	141 (25.2%)	146 (26.1%)
0.05 < z < 0.40	800	312 (39.0%)	176 (22.0%)	312 (39.0%)

the survey’s efficiency is small (Dilday et al. 2010) compared to the statistical precision of our data and it is not necessary for us to include the uncertainty in our analysis. We now turn to consider the host galaxies of these SN events.

4. Host Galaxy Determination and Derived Quantities

Here we describe the method used to identify the host galaxies and determine their characteristics, such as stellar mass and recent star-formation rate, for the 379 SNe Ia identified in §3. We also outline the comparison field sample used to describe the underlying galaxy population in our redshift range.

4.1. Host Galaxy Determination

Repeat imaging of SDSS Stripe 82 has enabled the coaddition of images into a deep stacked image (Abazajian et al. 2009). The stack ranges from 20 to 40 individual images (depending on sky position) in all 5 SDSS filters (*ugriz*) and is roughly 2 magnitudes deeper than a single epoch SDSS image. To determine the host galaxy for each SN in our sample, we match the SN positions with SDSS galaxies detected in this deep stacked image within a 0.25 arcminute radius. We require that the host galaxy has an SDSS model magnitude (Stoughton et al. 2002) in the range $15.5 < r < 23.0$ to ensure

robust photometry. This magnitude cut is conservative, but applied to ensure that the SDSS-II SN pipeline is able to accurately distinguish between stars and galaxies in the deep stacks. The magnitude limits remove 10% of our SNe with either unobserved or too faint hosts. We then visually scan each host galaxy, using images with and without the supernova present to ensure that our host galaxy association is accurate. In six cases, at low redshift, where the host is extended or resolved into multiple objects, we select by hand a more likely object as the host galaxy. Of the 379 SNe Ia candidates identified in §3, 342 have a valid host galaxy identification, of which 197 (58%) are spectroscopically confirmed to be SNe Ia, and 87 (25%) are spectroscopically unconfirmed but have a host galaxy spectroscopic redshift. The remaining 58 objects are classified to be SNe Ia through their photometry alone. Of the 37 candidates that lack a valid host galaxy, 29 (78%) have a host galaxy candidate with $r > 23.0$ and 8 (22%) have no host candidate within a 0.25 arcminute radius.

4.2. Derived Host Galaxy Properties

Having identified the host galaxy position and magnitudes for 342 SNe Ia candidates, we now determine their stellar mass and recent star-formation rate.

There are several methods to infer galaxy properties from broad-band photometry. A simple cut

on the color of the galaxy can be used to infer its spectral type (Strateva et al. 2001) and the UV flux can provide an estimate of the recent star-formation rate (Donas et al. 1987). These simple methods are able to differentiate between galaxies with markedly different levels of star-formation activity, but struggle with galaxies with similar colors because multi-band photometry is not used (Baldry et al. 2006). Therefore, we fit our multi-band photometry to a set of Spectral Energy Distributions (SEDs) and use the best-fit template to determine the galaxy parameters. This technique is widely used for photometric redshift estimates (Bolzonella et al. 2000; Le Borgne & Rocca-Volmerange 2002; Oyaizu et al. 2008).

4.2.1. SED Fitting

The method used here is consistent with that of Sullivan et al. (2006), who studied the SN Ia rate as a function of host galaxy properties at high redshift, allowing our results to be compared within the same framework. A discussion on how the different redshift ranges covered by this analysis and that of Sullivan et al. (2006) may affect our host galaxy derived properties is given in Appendix E.

We use the SEDs produced by the PÉGASE.2 galaxy spectral evolution code (Fioc & Rocca-Volmerange 1997; Le Borgne et al. 2004). These templates have been used extensively in the literature to constrain the evolution of galaxies, particularly at high redshift (Glazebrook et al. 2004; Grazian et al. 2006). We use the set of 8 evolutionary tracks listed in Table 1 of Le Borgne & Rocca-Volmerange (2002) (excluding the starburst template), and assume a Kroupa (2001) Initial Mass Function (IMF). In these scenarios, star-formation rate is determined using the relationship $\text{SFR} = \nu \times M_{\text{gas}}$, where ν ranges from 0.07 to 3.33 Gyr^{-1} , and M_{gas} is the density of gas in solar masses. Extinction due to dust is modelled internally, with a King (1980) profile used for the Elliptical template, and a plane-parallel slab geometry is used for the spiral and irregular templates. Each of the 8 evolutionary scenarios is evolved over 69 time steps, each one corresponding to a different galaxy age, making a total of 552 template SEDs.

These SEDs are convolved with the SDSS filter responses (Fukugita et al. 1996) and fitted to the galaxy fluxes (calculated from model magnitudes after correcting for Galactic dust absorption from

Schlegel et al. (1998) and AB-system offsets) using the Z-PEG photometric redshift code (Le Borgne & Rocca-Volmerange 2002). We keep the redshift of the SN host galaxies fixed to the spectroscopic redshift (from either the SN or host galaxy) or the photometric redshift determined by MLCS2k2. Applying a redshift constraint eliminates the color uncertainty due to the cosmological redshift. As dust is included internally in the SEDs no dust correction is applied in the fitting process. We assume a default Λ CDM cosmology ($\Omega_M = 0.3, \Omega_\Lambda = 0.7$) and consider only templates that are younger than the age of the Universe at the fitted redshift.

The best-fit template is determined through a χ^2 minimization using all 5 SDSS filters. The total stellar mass of each galaxy is determined by integrating the star-formation history of the best-fitting SED and subtracting the mass of stars that have died. We characterize recent star-formation with a mean star-formation rate, since the instantaneous star-formation rate is difficult to estimate without high-resolution spectroscopic data. We use the result of Sullivan et al. (2006), who found that averaging the star-formation rate over a period of 0.5 Gyr can be accurately recovered by the PÉGASE.2 SEDs, without introducing significant systematic uncertainties, especially for galaxies where the redshift is unknown.

Uncertainties in the galaxy properties are determined from the range spanned by the SEDs satisfying $\chi^2 \leq \chi_{\text{min}}^2 + 1$. We consider errors on the galaxy fluxes from the coadded image, with a minimum error as given in Blanton & Roweis (2007). The stellar mass and recent star-formation rate for the 342 host galaxies used in this analysis is given in Table 9.

4.3. Comparison Field Sample

To determine how our SN sample relates to the underlying galaxy population in our redshift range, we require a sample of galaxies that is representative of the general galaxy population. For this sample, we use galaxies detected in the deep stacks described in §4.1. We consider galaxies identified in the SDSS-II SN Survey region with $15.5 < r < 23.0$. This cut also removes the possibility of variable limiting magnitudes across the image.

We determine the stellar masses and recent

star-formation rates for each galaxy in this sample using the same method as for the host galaxy sample except that the redshift is a free parameter to be determined by the Z-PEG fit. We require that the fitted redshift must lie in the redshift range $0 < z < 2$. The additional freedom allowed in determining the redshift for the field galaxies can result in large error bars on the derived photometric redshift, stellar mass and star-formation rate estimates. In extreme cases, there can be two or more distinct best-fit template solutions, resulting in more than one photometric redshift estimate and spectral type. In these cases, the galaxy is excluded from our analysis because the spectral classification and derived galaxy properties are ambiguous. To match the host galaxy population, we consider the $\sim 750,000$ galaxies with $0.05 < z < 0.25$.

4.4. Correcting For Incompleteness in the Field Sample

The comparison field sample is magnitude limited, and thus becomes increasingly incomplete at higher redshifts, with only the brightest galaxies observed at higher redshifts. Galaxies with a given absolute magnitude (and spectral type) will pass the apparent magnitude selection criteria ($15.5 < r < 23.0$) at different redshifts, which may be less than the full survey range ($0.05 < z < 0.25$). To correct for this effect, we use the V_{\max} method (Schmidt 1968; Felten 1976). Using the best-fitting SED for each field galaxy, we calculate its absolute magnitude and k-correction, and determine the redshift limits at which it would satisfy $15.5 < r < 23.0$. Whenever the redshift range is less than the total survey range ($0.05 < z < 0.25$), we weight the galaxy by $V_{\text{survey}}/V_{\max}$, where V_{\max} is the co-moving volume for which each galaxy will remain within our survey’s magnitude limits, and V_{survey} is the co-moving volume of the SDSS-II SN survey, *i.e.* for a redshift range, $0.05 < z < 0.25$ and constant for each galaxy in our sample. 83% of the field galaxies in our sample have redshift limits larger than that of the SDSS-II SN survey, and are not affected by this correction. The remaining 17% of field galaxies are on average weighted by a value of 4.98. Since this form of incompleteness will affect both the comparison field sample and host galaxy sample, this incompleteness correction is applied

to both, although only 3 of the 342 host galaxies in our sample are affected by this correction.

4.5. Systematic Uncertainties

Systematic uncertainties in our derived galaxy properties can arise from many sources including the wavelength coverage of the SDSS filters, our decision to use the PÉGASE.2 SEDs, our choice of IMF, the accuracy of the photometric redshifts for the comparison field sample, the accuracy of the PÉGASE.2 stellar mass estimates, and the ability of PÉGASE.2 to accurately recover the stellar masses and star-formation rates for a sample of simulated galaxies. All these systematic errors are discussed further in Appendix A, B, C, D and E.

In Appendix A, we show that the PÉGASE.2 SEDs primarily use the color of a galaxy as a proxy to infer its spectral type. The reddest galaxies are classified as passive galaxies, with the bluest galaxies considered highly star-forming. Moderately star-forming galaxies are distributed between passive and highly star-forming galaxies, spanning a large range of color.

In Appendix B, we investigate the accuracy of the PÉGASE.2 photometric redshift estimates for our field sample. We find a mean offset in redshift of $\Delta z = 0.03$, with the photometric redshift estimate being smaller than the known spectroscopic redshift. This redshift error results in an error in stellar mass of $\Delta \log M = 0.22 M_{\odot}$. In Appendix C we show the effect that applying this offset to our data would have on the results presented in §6 and show that they are consistent. This offset provides us with an estimate of our systematic uncertainty, but due to a lack of understanding of the cause of this offset, it is not applied to our nominal analysis.

Appendix D studies how the stellar mass and star-formation rate estimates from PÉGASE.2 for our host galaxy sample compare to those determined using the spectral features of galaxies. We consider a sample of SDSS galaxies that have spectroscopically measured stellar masses and star-formation rates (Brinchmann et al. 2004; Kauffmann et al. 2003) and compare these to estimates determined in our analysis. We find that the stellar masses are recovered, with no significant offset, but there is a mean offset in the star-formation rate of $\Delta \log \text{SFR} = 0.12 M_{\odot} \text{yr}^{-1}$.

However, Brinchmann et al. (2004) measure the “instantaneous” (present day) star-formation rate instead of our “recent” star-formation rate, which is averaged over the last 0.5 Gyr, so the two quantities are not directly comparable.

In Appendix E we consider how the rest-wavelength coverage of the SDSS filter set affects our stellar mass estimates. With increasing redshift, the SDSS filters will sample a different rest wavelength ranges. This can be particularly important for systems with a variety of stellar populations, such as merging galaxies. To examine the sensitivity to our wavelength coverage, we repeat the determination of stellar masses and star-formation rates using only three or four of the five SDSS filters. We find an increased scatter in the results, but no overall bias in the stellar mass or star-formation rate estimates. This is particularly encouraging, because it suggests that the comparison of our galaxy properties with those of Sullivan et al. (2006) will not be affected by the different cosmological redshifts of the two surveys.

5. Host Galaxy Properties

In §3 we defined a sample of homogeneously selected SNe Ia, and, in §4, determined a host galaxy for each object. Having estimated their stellar mass and recent star-formation rate, we now analyze these derived properties, and how they relate to the supernova rate.

Figure 2 shows the distribution of our host galaxy sample in stellar mass and star-formation rate (SFR). Galaxies are shown in three categories, highly star-forming (blue), moderately star-forming (green), and passive (red). The highly and moderately star-forming galaxies are separated by their specific star-formation rate (sSFR): the star-formation rate per unit stellar mass (Guzman et al. 1997; Brinchmann & Ellis 2000; Brinchmann et al. 2004; Sullivan et al. 2006). We followed Sullivan et al. (2006) in choosing $\log s\text{SFR} = -9.5$ as the arbitrary division between highly and moderately star-forming as indicated by the dashed line on Figure 2. Highly star-forming galaxies are using a significant proportion of their stellar mass to form new stars and their stellar populations are expected to be dominated by young, massive stars. Galaxies classified as moderately star-forming are likely

to be dominated by an older, more evolved population of stars. Passive galaxies have a nominal $\text{SFR} = 0$, but for display purposes, are randomly distributed in red on Figure 2 around $\log \text{SFR} = -3.5$. The average stellar mass of a passive galaxy is $\log M = 10.52 M_{\odot}$, considerably more massive than star-forming galaxies, which average $\log M = 9.91 M_{\odot}$, consistent with other observations of the local universe (Taylor et al. 2009).

Of the 342 galaxies in our sample, 80 (23%) are classified as passive galaxies, 139 (41%) have moderate levels of star-formation activity and 123 (36%) are highly star-forming.

In Figure 2, we note a “ridge line” of galaxies, which are classified as moderately star-forming, but have the lowest possible values of sSFR allowed. A dashed-dotted line is shown on Figure 2 to highlight this population of galaxies. 78% of these galaxies are best-fit by the lenticular S0 (scenario), with the remaining 22% being best-described by the elliptical template. In comparison 52% of the remaining moderately star-forming galaxies are best-fit by the S0 scenario. In Appendix A we show the color-magnitude diagram, and conclude that these galaxies lie at the edge of the distribution of the moderately star-forming galaxies but appear to be distinct from the passive galaxies. Thus, we do not remove these galaxies from our analysis. We will show later through a Monte-Carlo approach that removing these galaxies from our sample do not affect our major conclusions.

6. SN Ia Rate

We now turn to looking at how the supernova rate depends on the galaxy properties of total stellar mass and recent star-formation for passive and star-forming galaxies.

6.1. SN Ia Rate as a Function of Host Galaxy Stellar Mass

According to the standard model of galaxy formation, passive galaxies are primarily comprised of old, low mass stellar systems that evolve without forming new stars. It is reasonable to suppose that the SN Ia population in passive galaxies could only occur as a result of a process with a delay time that is long compared to the age of the galaxy. If

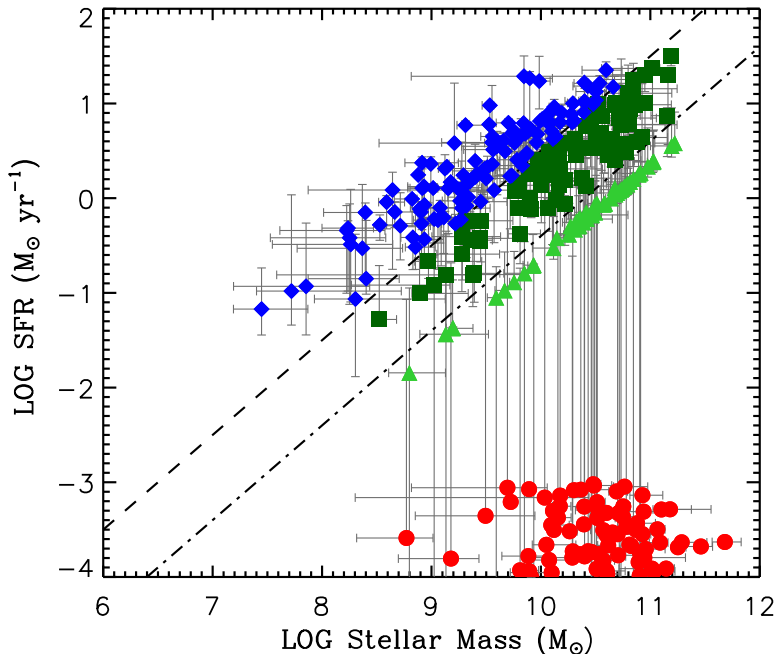


Fig. 2.— The distribution of stellar mass & SFR for the 342 SN host galaxies. Highly star-forming galaxies are shown as blue diamonds and passive galaxies as red circles. Moderately star-forming galaxies are plotted in green, with light green triangles indicating the “ridge line” of galaxies discussed in the text and Appendix A, and the remaining population plotted as dark green squares. The dashed-dotted line highlights this split. Passive galaxies have $\text{SFR} = 0$ but are shown here as randomly distributed in the range $-4 < \log \text{SFR} < -3$. The dashed line indicates the split used to distinguish highly star-forming galaxies from those with moderate levels of star-formation activity. .

that is the case, then the number of SN Ia’s occurring in these environments could be expected to be proportional to the host galaxy stellar mass. On the other hand, if the delay time is only comparable to the age of the galaxy, there could be a more complicated dependence based on the details of the star-formation history.

To measure the stellar mass dependence with the SDSS data, we split both our host galaxy sample and comparison field sample into passive and star-forming galaxies. The samples are binned by their stellar mass, with both the host galaxy and field sample weighted for incompleteness using the $1/V_{\text{max}}$ correction, and the efficiency correction applied to the host galaxy sample. Each host galaxy is weighted by $1/\epsilon$, the survey efficiency at the redshift of the SNe given the year it was observed. The efficiency correction ranges

between 1.4 and 2.6, with a mean weighting of 1.9 for each host galaxy. By dividing the number of host galaxies by the corresponding number of field galaxies, and including a correction for the survey’s observing period, we can determine how the rate of SNe Ia varies as a function of the stellar mass of their host galaxy. Figure 3 shows the SN Ia rate for both the passive and star-forming galaxy samples. It is clear that the rate of SNe in all types of galaxies depends on the stellar mass. We also see that the relationship between the SN Ia rate and stellar mass is different for passive galaxies and star-forming galaxies in the SDSS data.

The data are fit to a linear function in log-space, corresponding to a power law dependence of SN rate on stellar mass as shown on Figure 3. A linear dependence on stellar mass would result in a slope of unity. The error bars shown and fitting errors

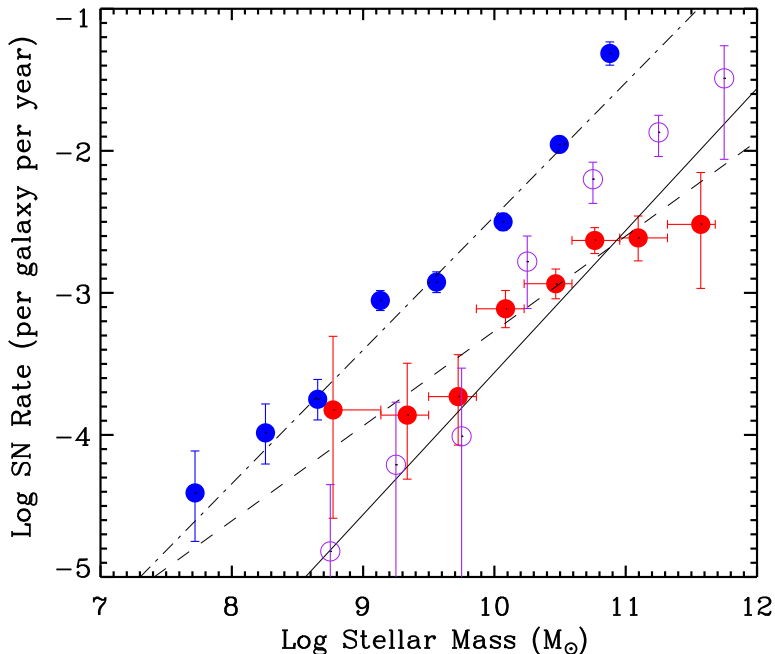


Fig. 3.— SN Ia rate as a function of host galaxy stellar mass. The values for star-forming (passive) galaxies are shown in blue (red). The data points, for passive galaxies, from Sullivan et al. (2006) are shown as open circles. The best-fitting lines for passive and star-forming galaxies are shown as dashed and dotted-dashed lines, respectively. Also shown is a fit (solid line) to the passive galaxies where the line slope is assumed to be one.

include statistical errors only. The uncertainty in galaxy stellar mass is discussed in §6.7. For passive galaxies, we find a best-fit slope of 0.67 ± 0.15 (with χ^2 -statistic (χ^2) = 2.30 for 6 degrees of freedom) compared to a value of 0.94 ± 0.08 (χ^2 = 9.28 for 6 degrees of freedom, denoted as $n_{\text{star-forming}}$) for star-forming galaxies. The value for passive galaxies is incompatible (at the 2.2σ level) with a linear relationship, as favored by Sullivan et al. (2006), who found a slope of 1.10 ± 0.12 using the SNLS data at higher redshift.

Figure 3 also shows the results for passive galaxies from Sullivan et al. (2006) as open circles. We see that the SDSS galaxy sample contains fewer SNe Ia in high mass passive galaxies than SNLS and more SNe Ia in low mass passive systems. While the two analyses should be directly comparable, the galaxy population is expected to evolve between $z \sim 0.75$ and $z \sim 0.2$. However, it does not seem that galaxy evolution can explain

these differences as more massive galaxies should be found in the local universe. In addition, we note that the SDSS analysis finds a larger slope for star-forming galaxies compared to passives, while the opposite is seen in the SNLS data, who find values of $n_{\text{star-forming}} = 0.66 \pm 0.08$ and 0.74 ± 0.08 , for moderately and highly star-forming galaxies respectively. Li et al. (2010) find the slope is independent of host galaxy type, with a value of 0.5 providing a good fit in all cases.

6.2. Parameterizing the SN Ia Rate

The data in Figure 3 indicate that the SN Ia rate depends on galaxy stellar mass, but also that the rate depends on whether the galaxy is actively forming stars. A two-component model was considered by Mannucci et al. (2006), and Scannapieco & Bildsten (2005), who modelled the SN Ia rate of a galaxy to consist of a “delayed” component, with a long delay time that

is driven by the stellar mass of the galaxy, and a “prompt” component, with short delay times that is caused by the formation of new stars. The model assumes that the “delayed” component is proportional to the stellar mass independent of the galaxy age and star-formation history, and that the “prompt” component time scale is short compared to changes in the star-formation rate. These assumptions result in an expression whose parameters can be determined from data as was done by Sullivan et al. (2006). In detail, the SNR_{Ia} can be written as;

$$\text{SNR}_{\text{Ia}}(t) = A \times M(t) + B \times \dot{M}(t), \quad (1)$$

where $\text{SNR}_{\text{Ia}}(t)$ is the explosion rate of SNe Ia at time t , $M(t)$ is the stellar mass of a galaxy, $\dot{M}(t)$ is the rate of change of stellar mass, and A and B are constants determined from the data and have units $\text{SNe yr}^{-1} M_{\odot}^{-1}$ and $\text{SNe yr}^{-1} (M_{\odot} \text{ yr}^{-1})^{-1}$, respectively. We assume $\dot{M}(t)$ is equal to the star-forming rate (SFR) (averaged over the previous 0.5 Gyr) as discussed in §4.2. While the model is, in principle, valid for all t , our SN rate measurements apply only to the current era and we will suppress the dependence on t . This model is commonly known as the “A+B” model for the supernova rate and assumes that the SN Ia rate is linearly dependent on both the stellar mass of a galaxy and its star-formation rate. However, in §6.1 we showed that for passive galaxies (whose SN Ia rate will be purely dependent on stellar mass in this parameterization), a linear dependence was not favored by the SDSS dataset. We therefore generalize Equation 1 to,

$$\text{SNR}_{\text{Ia}} = A \times M^{n_{\text{M}}} + B \times \dot{M}^{n_{\text{SFR}}}, \quad (2)$$

where n_{M} , n_{SFR} , A and B are constants to be determined from the data. Since passive galaxies have $\dot{M} = 0$, we can apply the results of §6.1 to conclude $n_{\text{M}} = 0.67 \pm 0.15$. The straight line fit to the passive galaxies yields $\log A = -9.95 \pm 0.68$ or $A = 1.11_{-0.88}^{+4.17} \times 10^{-10} \text{SNe yr}^{-1} M_{\odot}^{-1}$. If we assume $n_{\text{M}} \equiv 1$, we find a value of $\log A = -13.56 \pm 0.08$ or $A = 2.75_{-0.47}^{+0.57} \times 10^{-14}$, which differs at 2.1σ with the value of $A = 5.3 \pm 1.1 \times 10^{-14}$ found using the SNLS dataset.

While the above parameterization of the SN Ia rate uses the stellar mass and the recent star-formation rate, other galaxy properties can be considered, such as the metallicity, age and level of

extinction. Gallagher et al. (2005) find qualitative evidence suggesting that the progenitor age is a possible source of diversity in SNe Ia properties. However, there is a degeneracy between the age of a galaxy, and its metallicity, which is extremely difficult to break using broad-band photometry. We thus confine ourselves to considering the stellar mass and star-formation rates of our host galaxies in this analysis, but note that with improved stellar population models, a larger wavelength coverage and galaxy spectra, it may be possible to break this degeneracy. Using SDSS-II SNe, Gupta et al. (2011) attempt to break this degeneracy by using multi-wavelength photometry to better constrain the ages of their SN Ia host galaxies while D’Andrea et al. (2011) and Konishi et al. (2011) use spectral features to determine the metallicities of their host galaxies.

6.3. SN Ia Rate as a Function of Host Galaxy Mean Star-formation Rate

We now consider the star-forming galaxies to determine B and n_{SFR} . We bin the host galaxy and comparison field sample in star-formation rate, and as in §6.1, correct both samples for incompleteness, using the SN efficiency for the host galaxy sample and the $1/V_{\text{max}}$ correction for both the host galaxy and comparison field samples. The SN Ia rate is shown (blue diamonds) as a function of SFR in Figure 4. We want to determine the excess SN Ia rate due to recent star-formation activity assuming that the term proportional to stellar mass is the same for star-forming and passive galaxies. The portion due to the stellar mass term is calculated using Equation 2, and shown on the figures (green points) as are the SN Ia rates after the stellar mass term has been subtracted (red points). The left panel of Figure 4 uses our best-fit line with slope $n_{\text{M}} = 0.67$ while the right panel uses the fit where the slope is fixed at $n_{\text{M}} \equiv 1$.

The observed SN Ia rate depends strongly on recent star-formation and greatly exceeds the rate in passive galaxies with identical stellar mass. We find $n_{\text{SFR}} = 0.96 \pm 0.07$ and $\log B = -2.81 \pm 0.04$ ($B = 1.55_{-0.15}^{+0.16} \times 10^{-3} \text{SNe yr}^{-1} (M_{\odot} \text{ yr}^{-1})^{-1}$) with $\chi^2 = 1.58$ for 6 degrees of freedom when $n_{\text{M}} = 0.67$. When $n_{\text{M}} \equiv 1$ is assumed, we find $n_{\text{SFR}} = 0.98 \pm 0.08$, and $\log B = -2.85 \pm 0.05$ ($B = 1.42_{-0.15}^{+0.17} \times 10^{-3} \text{SNe yr}^{-1} (M_{\odot} \text{ yr}^{-1})^{-1}$) with $\chi^2 = 1.52$ for 6 degrees of freedom. The lack of

sensitivity to the value of $n_M = 0.674$ follows because the stellar mass term is always small compared to the star-forming term.

Our best-fit to Equation 2, is therefore

$$\begin{aligned} \text{SNR}_{\text{Ia}} = & 1.11_{-0.88}^{+4.17} \times 10^{-10} M^{0.67 \pm 0.15} \\ & + 1.55_{-0.15}^{+0.16} \times 10^{-3} \dot{M}^{0.96 \pm 0.07}. \end{aligned} \quad (3)$$

As noted previously, the analysis of Sullivan et al. (2006) in the redshift range $0.2 < z < 0.75$ preferred a SN Ia rate linearly dependent to the stellar mass of a galaxy. If we assume $n_M \equiv 1$ and $n_{\text{SFR}} \equiv 1$, we find,

$$\text{SNR}_{\text{Ia}} = 2.75_{-0.47}^{+0.57} \times 10^{-14} M + 1.40_{-0.13}^{+0.14} \times 10^{-3} \dot{M}. \quad (4)$$

For comparison, Sullivan et al. (2006) find values of $A = 5.3 \pm 1.1 \times 10^{-14} \text{SNe yr}^{-1} M_{\odot}^{-1}$ and $B = 3.9 \pm 0.7 \times 10^{-4} \text{SNe yr}^{-1} (M_{\odot} \text{yr}^{-1})^{-1}$. Our value of A is 2.1σ lower, while the values of B are inconsistent at 3.5σ , indicating that recent star-formation activity plays a more significant role in determining the overall SNe Ia rate for our sample. This result is consistent with models of how galaxies evolve through cosmic time. Observations suggest, that at high redshift ($z = 0.75$), the rate of star-formation is far higher than in the local Universe. Combining this with measurements suggesting that the SN Ia rate increases slowly as a function of redshift, suggests that recent star-formation activity is more significant in determining the SN Ia rate at low redshift. The methodology used in this analysis is similar to that used in Sullivan et al. (2006), and has been significantly tested (§A, §B, §C, §E).

6.4. Bivariate Fitting

Thus far we have used only the passive galaxies to determine the A term and then used the star-forming galaxies to determine the B term, while keeping A fixed. A more sophisticated method is to constrain the parameters simultaneously using all galaxy types, thus making optimal use of the data. We bin the host galaxy and comparison field sample in the stellar mass and star-formation plane, and correct for incompleteness. By dividing the number of host galaxies in each bin by the corresponding number of field galaxies, we are able to determine the SN Ia rate in each bin of stellar mass

and star-formation rate. We consider several variations on Equation 2. First, we consider the case where $B \equiv 0$, *i.e.* the SN Ia rate is purely dependent on stellar mass, and n_M is a free parameter. In this case, we find $A = 1.08 \pm 0.18 \times 10^{-10}$ and $n_M = 0.68 \pm 0.005$, in agreement with the result found in §6.1. However, this is a poor fit to the data, and allowing $B \neq 0$ but assuming $n_{\text{SFR}} \equiv 1$ reduces the χ^2 from 347 for 42 degrees of freedom to 142 for 41 degrees of freedom, and yields values of n_M , A , and B consistent with those found in §6.3. Finally, we allow n_{SFR} to vary and find $n_{\text{SFR}} = 1.00 \pm 0.05$ with $\chi^2 = 142$ for 40 degrees of freedom, a negligible improvement.

We thus conclude that our data is consistent with a linear dependence on star-formation rate. Our fiducial result using bivariate fitting is

$$\begin{aligned} \text{SNR}_{\text{Ia}} = & 1.05 \pm 0.16 \times 10^{-10} M^{0.68 \pm 0.01} \\ & + 1.01 \pm 0.09 \times 10^{-3} \dot{M}^{1.00 \pm 0.05}. \end{aligned} \quad (5)$$

This is in good agreement with the values found in §6.1 and §6.3.

6.5. SN Ia Rate as a Function of Specific Star-Formation Rate

The results from §6.1, §6.3 and §6.4 have shown that the SN Ia rate depends on both the galaxy stellar mass and star-formation rate, with star-formation rate dominating the SN Ia rate. Here, we study how the SN Ia rate is related to host galaxy type. To determine this, we bin the host galaxy and comparison field samples according to their value of sSFR. Both samples are corrected for incompleteness, and the total stellar mass of the field sample is calculated. By dividing the incompleteness corrected number of host galaxies by the total stellar mass of the field sample, we are able to determine the SN Ia rate per unit stellar mass as a function of sSFR. As noted in §5, sSFR is a way of distinguishing between galaxy types, with galaxies with low values of sSFR being primarily large galaxies that are using a small fraction of their total stellar mass to form new stars, while those with larger levels of sSFR are starburst galaxies, or galaxies that are using a significant fraction of their stellar mass to form new stellar systems.

Figure 5 exhibits the rate of SNe Ia per unit stellar mass in star-forming galaxies as a function of sSFR. The rate increases with sSFR, reaching

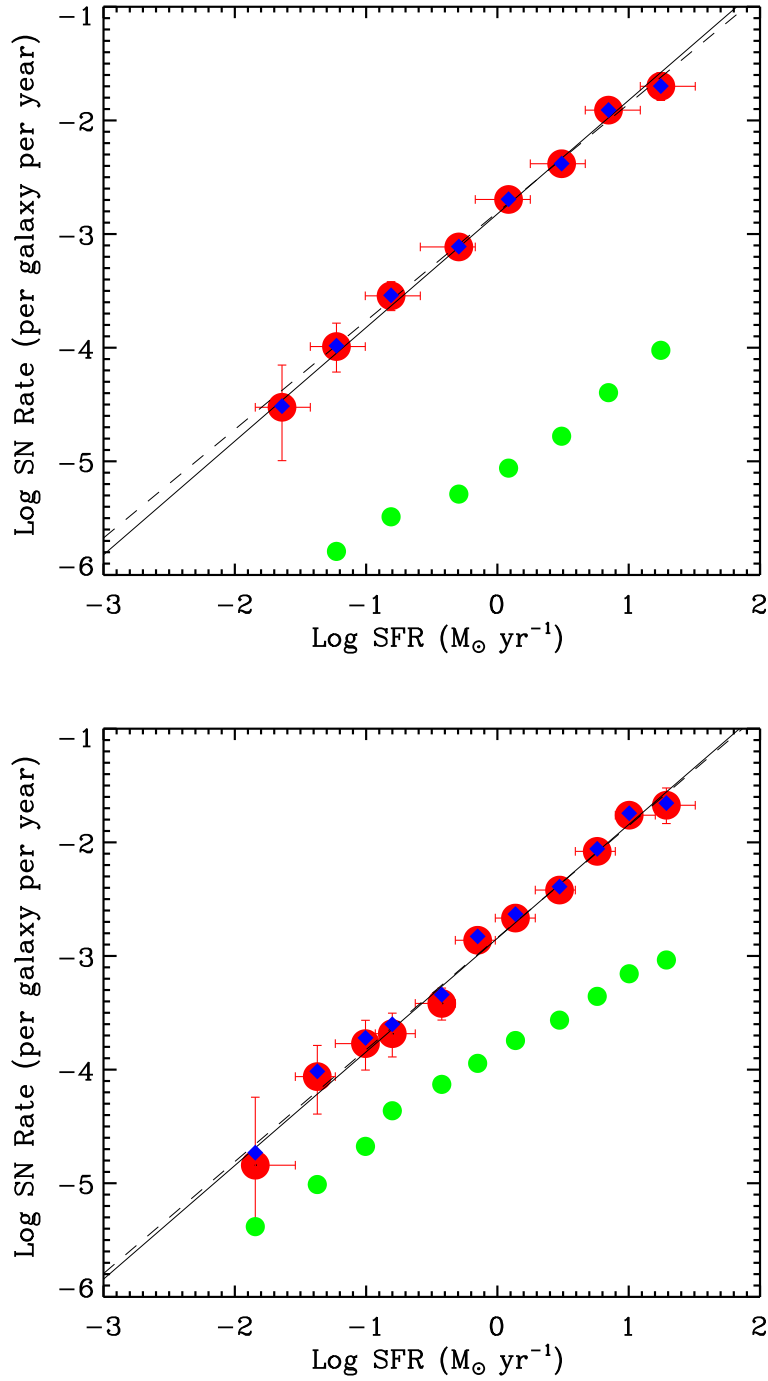


Fig. 4.— SN Ia rate as a function of host galaxy star-formation rate. *Left panel:* Green points indicate the expected rate of SNe Ia due to the stellar mass of each galaxy, using the values of n_M and A as determined in §6.1. Blue diamonds show the observed rate of SNe Ia per galaxy per year, while the red points are the excess (*i.e.* the difference between the blue and green values). A best-fitting line (dashed), and best-fitting line with unit slope (solid) is also shown. *Right panel:* Identical, except a value of $n_M \equiv 1$ is assumed.

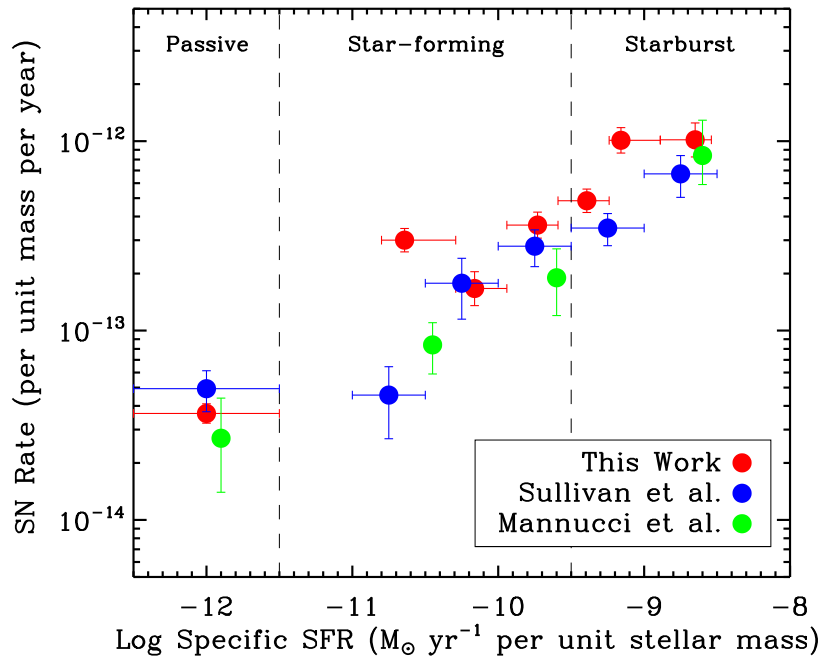


Fig. 5.— The SN Ia rate per unit stellar mass per year as a function of host galaxy specific star-formation rate (sSFR). The red points are those determined by the SDSS analysis, blue points are those from Sullivan et al. (2006), while points shown in green are measurements at low redshift made by Mannucci et al. (2005), where the magnitude and color of the host galaxy have been used to determine the host galaxy stellar mass and star-formation rate. The horizontal errors on the SDSS data indicate the bin width while the horizontal positions represents the mean of the data in that bin. The positioning of green points on the x-axis is somewhat uncertain since precise values for sSFR were not given. Passive galaxies have $sSFR = 0$, but are shown on this graph, with $\log sSFR \simeq -12$.

an increased factor of ~ 30 for starburst galaxies compared to passive galaxies. The measurements of this work are in excellent agreement with those found at higher redshift (Sullivan et al. 2006) and in the local universe (Mannucci et al. 2005), indicating that this relationship holds for all redshifts that have been studied. The SDSS data, however, has a point that appears to disagree with the other data and the generally linear trend of increasing SN Ia rate with sSFR. This point corresponds to the galaxies highlighted in §5 as being on the edge of the moderately star-forming galaxies. Appendix A considers these objects, and determines that while there was a possible ambiguity in the classification of these objects, they constitute a distinct population that lie between passive and star-forming galaxies. Any contamination

by passive galaxies would tend to reduce the rate, but the measurement appears to be high compared to previous measurements. Another possibility is that we might have underestimated the number of weakly star-forming field galaxies but there is no evidence that this is the case based on the comparison in Appendix D.

6.6. The Effect of our Selection Criteria

We have studied how the SN Ia rate is related to the host galaxy properties for the SDSS sample. However, as discussed in §3.1, the sample constructed for this analysis is comprised of SNe Ia that have not all been spectroscopically confirmed and thus may be contaminated by non-SN Ia events. Our analysis has also used an efficiency correction, which is increasingly important

towards the edge of our redshift range, and thus can cause uncertainties in our results.

Table 3 shows the results that we obtain using various subsets of our SN Ia sample. In the two left-hand columns we show fits for the spectroscopically confirmed and unconfirmed portions of our sample. In the three right-most columns we show the results for three different redshift ranges. The spectroscopically confirmed and unconfirmed subsamples are, of course, incomplete, so the A and B parameters will necessarily be smaller than for the full sample. The results for n_M and n_{SFR} , however, should be comparable.

From Table 3 we see that the spectroscopically confirmed sample is fit by $n_M = 0.873 \pm 0.273$, consistent with the combined result but also consistent with $n_M = 1$. This value of n_M may be due to the lower proportion of passive galaxies in this sample and a bias against more luminous and thus massive galaxies in the spectroscopic selection. This bias is caused by a targeting against probable SNe Ia that occur in the centres of luminous galaxies, making them difficult to identify spectroscopically. As the redshift limit considered is decreased, resulting in a more complete sample, the value of n_M is stable and shows no trend towards one (although the errors increase rapidly as the sample size is reduced). The value for $\log A$ when we assume $n_M \equiv 1$ is consistent for all the redshift ranges (when n_M is a free parameter, it is highly degenerate with $\log A$). Table 3 also shows that the value of n_{SFR} is not influenced by the inclusion of non-spectroscopically confirmed SNe Ia nor the redshift range.

Table 3 also shows how our selection criteria affects the dependence that the SN Ia rate has on the star-formation rate. We showed in §6.3 and §6.4, that the SN Ia rate depends approximately linearly on the recent star-formation rate. The subsamples displayed in Table 3 are all consistent and there is no hint on any deviation from $n_{\text{SFR}} \sim 1$. A value of $\log B \sim -2.85$ is valid for all redshift ranges considered.

Finally, we study the results of §6.5. The “passive rate” in Table 3 is the rate per unit stellar mass per year in passive galaxies, as shown in Figure 5, while the “starburst rate is the corresponding rate for galaxies with the highest levels of sSFR (sSFR > -9.5). The values of both the passive and starburst rates are consistent independent of

the redshift limit used and are consistent with the sum of the spectroscopically confirmed and unconfirmed samples. In all cases, the rate of SNe Ia per unit stellar mass in highly star-forming galaxies is significantly higher (by a factor of ~ 30) than that seen in passive galaxies.

The fit parameters shown in Table 3 do not evolve across our redshift range. Since any evolution would be unexpected due to the small range in cosmic time covered by our analysis, it is reassuring to note that our results are insensitive to the redshift interval that is chosen. The only parameter that significantly changes with redshift is the proportion of passive galaxies found. This may simply reflect observations that SNe Ia in passive galaxies are fainter than their star-forming counterparts (see §7 for an analysis with the SDSS sample) and thus are not observed at higher redshifts by the SDSS-II SN survey.

In Table 3 we considered separately the spectroscopically confirmed and unconfirmed SNe Ia and various redshift ranges on our conclusions. However, there are several other uncertainties that can arise as part of our selection criteria and analysis. We also investigated the effect of using different priors on A_V when determining the sample of SNe Ia, by using a flat prior and a positive prior ($A_V \geq 0$). The various priors produce results that are entirely consistent with those found previously. In the determination of n_M and n_{SFR} we have performed linear fits to the log-log plots, but it is also possible to fit to the power law form directly. These fits are consistent with our linear fits to the logarithms. We have also considered various bin sizes for each stage of our analysis and find that our results are unaffected. We also considered the possibility that our results may depend on a specific, anomalous year with the SDSS-II SN survey or may vary as a function of position on the sky. We split the host galaxy sample by both year and position but found no variation on our final results. Finally, we considered the effect of modelling ϵ , the survey efficiency, as a function of redshift, A_V and Δ , to account for the observation that passive galaxies host fainter, higher Δ , SNe than star-forming galaxies (§7), which could result in the survey efficiency varying as a function of host galaxy type. This additional correction, which has not been applied for other previous analyses, produces results that are entirely consis-

TABLE 3

EFFECT OF OUR SELECTION CRITERIA ON THE RESULTS DESCRIBED IN §6.1, §6.3 AND §6.5

Parameter	Nominal Result	Confirmed ^g	Phot-ID ^h	$z < 0.20$	$z < 0.16$	$z < 0.12$
No. Hosts	342	197	145	196	103	36
% Confirmed SNe	57.6	100.0	0.0	67.9	79.6	97.2
n_M	0.67 ± 0.15	0.87 ± 0.27	0.43 ± 0.41	0.66 ± 0.20	0.62 ± 0.26	0.62 ± 0.93
$n_{\text{star-forming}}$	0.94 ± 0.08	0.93 ± 0.11	0.92 ± 0.12	0.82 ± 0.09	0.82 ± 0.15	0.77 ± 0.28
$\log A$ ^a	-9.95 ± 0.68	-12.42 ± 0.89	-7.74 ± 1.04	-10.00 ± 0.76	-9.47 ± 0.86	-9.30 ± 1.37
$\log A$ ^b	-13.56 ± 0.08	-13.77 ± 0.11	-13.88 ± 0.13	-13.68 ± 0.11	-13.61 ± 0.14	-13.38 ± 0.24
n_{SFR} ^a	0.96 ± 0.07	0.95 ± 0.11	0.96 ± 0.15	1.00 ± 0.10	1.01 ± 0.12	1.14 ± 0.29
n_{SFR} ^b	0.98 ± 0.08	1.02 ± 0.11	0.98 ± 0.15	1.08 ± 0.12	1.07 ± 0.16	1.13 ± 0.47
$\log B$ ^c	-2.81 ± 0.04	-3.06 ± 0.06	-3.18 ± 0.07	-2.88 ± 0.06	-2.91 ± 0.08	-2.90 ± 0.15
$\log B$ ^d	-2.81 ± 0.04	-3.08 ± 0.05	-3.19 ± 0.07	-2.88 ± 0.05	-2.91 ± 0.08	-2.93 ± 0.15
$\log B$ ^e	-2.85 ± 0.04	-3.09 ± 0.06	-3.21 ± 0.07	-2.91 ± 0.06	-3.01 ± 0.10	-3.05 ± 0.18
% Passive galaxies	23.4	20.3	27.6	25.0	28.2	33.3
Passive Rate ^f	3.6 ± 0.6	1.7 ± 0.4	1.9 ± 0.5	2.8 ± 0.6	3.2 ± 0.9	3.8 ± 1.8
Starburst Rate ^f	124.7 ± 29.95	66.3 ± 24.2	35.3 ± 19.8	119.4 ± 56.7	96.0 ± 68.9	117.9 ± 109.0

^a n_M free, in units of $\text{SNe yr}^{-1} M_{\odot}^{-1}$ ^b $n_M \equiv 1$, in units of $\text{SNe yr}^{-1} M_{\odot}^{-1}$ ^c n_M and n_{SFR} free, $\text{SNe yr}^{-1} (M_{\odot} \text{yr}^{-1})^{-1}$ ^d n_M free and $n_{\text{SFR}} \equiv 1$, $\text{SNe yr}^{-1} (M_{\odot} \text{yr}^{-1})^{-1}$ ^e $n_M \equiv 1$ and $n_{\text{SFR}} \equiv 1$, $\text{SNe yr}^{-1} (M_{\odot} \text{yr}^{-1})^{-1}$ ^f $\times 10^{-14}$ per unit mass per year^gConsidering solely spectroscopically confirmed SN Ia^hConsidering solely photometrically typed SN Ia

tent with our fiducial result.

In order to study the robustness of our results, we have considered the effect of altering our selection criteria, in Table 3. We have shown that the inclusion of non-spectroscopically confirmed SNe Ia in our sample and varying our redshift range considered does not significantly change the values of A , B , n_M and n_{SFR}

6.7. The Effect of SED Errors on our results

For each host galaxy in our sample we have determined a value for its stellar mass and recent star-formation rate. Each of these measurements has an associated error that may allow galaxies to move between bins, and thus affect our fitted parameters. This may be especially important for the sample of galaxies with ambiguous classification, highlighted in §5 and Appendix A.

To quantify this effect on our results we use both a Monte-Carlo (MC) and Bootstrap (BP) approach. For the MC analysis 10,000 realizations of the host galaxy sample are made by draw-

ing from the estimated probability distribution for each host. We consider two cases: varying the stellar mass of each host galaxy and varying the stellar mass and star-formation rate. The second case allows galaxies to move from passive to star-forming and vice versa. Thus each of the MC samples consists of 342 host galaxies, each a variation on one specific host in the host galaxy sample.

For the BP analysis, we again obtain 10,000 realizations of the host galaxy sample, this time by selecting a host galaxy at random with replacement. This analysis allows each host galaxy to be selected on multiple occasions, probing the effect that outliers within the sample may have on our results. As with the MC approach we consider two cases: selecting the host galaxies before the sample has been separated into passive and star-forming datasets (thus allowing the relative proportions to change) and randomly sampling after separation, thus enforcing the same proportion of passive and star-forming galaxies in each dataset. The second approach tests the dependence of our results on a subset of objects, while the first case is par-

ticularly important for the sample of ambiguous galaxies, identified in §5, and investigates if they are likely to be predominantly passive in nature.

To determine how the SED uncertainties affect our overall conclusions, we determine the value of each parameter for each realization, and fit a Gaussian (which is observed to provide a good fit) to each distribution. This provides an estimate for the central values and systematic uncertainty in each case. Table 4 gives the values and associated errors for the parameters determined in this work for each of these four systematic tests.

Both the MC and BP analysis provide values for the parameters determined that are consistent with those found as our main result, as described in §6.1, §6.3, §6.5. In all cases considered the observed scatter from the MC and BP tests is smaller than the statistical uncertainty. We note that while the central value for n_M determined by the MC analysis is larger than our default result, it is still inconsistent with $n_M = 1$ at the 3.4σ level when the stellar mass is allowed to vary, and 2.9σ when galaxies are allowed to move from passive to star-forming.

We observe that the SN Ia rate per unit stellar mass in passive galaxies is consistent in all four cases considered. This implies that the sample of galaxies with ambiguous classifications (as noted in §5) do not affect our overall conclusions. In the MC where the stellar mass and star-formation rate are allowed to vary, these galaxies are able to move from moderately star-forming to passive where their error bars allow. However, we note that in this case, the SN Ia rate in passive galaxies is in fact lower than the observed value, suggesting that these galaxies are not passively evolving, and may have non-zero star-formation rates.

The systematic error bars determined by the MC and BP tests are sub-dominant to the statistical uncertainties obtained in §6.1, §6.3 and §6.5. Therefore, the uncertainties due to the SED fitting are not the major source of uncertainty. Extensive testing of the PÉGASE.2 SEDs is carried out in Appendix A, B, D and E. An offset is found in the photometric redshift estimates and associated stellar mass estimates for the comparison field sample used in our analysis. By assuming that this offset does not affect the star-formation rates for our galaxies, which are inferred through their color (which we determine in Appendix A),

we uniformly apply this offset to each galaxy in the comparison field sample, and recalculate the results of §6.1, §6.3 and §6.5. While we find some variation in the central values, our conclusions are unaffected. We find that the rate of SNe Ia as a function of stellar mass in passive galaxies is incompatible with a linear relationship in all cases considered. Having applied the determined offset we find a value of $n_M \sim 0.5$ is preferred, which is consistent with our result at the 1.2σ level. The excess rate of SNe Ia in star-forming galaxies is linearly proportional to the star-formation rate in all cases considered. We find some evidence for a lower SNe Ia rate per unit stellar mass in passive galaxies, than determined in §6.5, with a maximum difference of 2.2σ .

6.8. Comparison to other results

Throughout this analysis we have compared our results to that of Sullivan et al. (2006). We find a different dependence on stellar mass for the SN Ia rate, but agree that there is a strong dependence on the recent star-formation rate. In agreement with the results of Sullivan et al. (2006), we find that the SN Ia rate per unit stellar mass is greater in highly star-forming galaxies compared to passive galaxies, with an approximately linear dependence on sSFR except for one potentially anomalous point in the SDSS data. Different assumptions about the dependence of the SN Ia rate on stellar mass do not significantly alter our conclusions about its dependence on the recent star-formation rate.

A summary of how our results compare to those found by other studies is given in Table 5. Scannapieco & Bildsten (2005); Mannucci et al. (2005) also investigated the possibility that the SN Ia rate may be a two-component model, assuming $n_M = n_{\text{SFR}} = 1$. These analyses updated SN rates from Cappellaro et al. (1999), determining values of $A = 3.83_{-1.2}^{+1.4} \times 10^{-14} \text{SNe yr}^{-1} M_{\odot}^{-1}$, for SNe in E/S0 galaxies (which can be crudely associated with passive galaxies in this analysis) and either $B = 1_{-0.5}^{+0.6} \times 10^{-3} \text{SNe yr}^{-1} (M_{\odot} \text{yr}^{-1})^{-1}$ or $B = 2.3 \pm 1. \times 10^{-3} \text{SNe yr}^{-1} (M_{\odot} \text{yr}^{-1})^{-1}$, depending on whether the $z \leq 1.0$ core-collapse SN rate density (Dahlen et al. 2004) compared to the star-formation rate density (Giavalisco et al. 2004), or the population of SNe Ia found in blue ($B - K$) galaxies is used to model the SN Ia rate in star-

TABLE 4

EFFECT OF OUR SED UNCERTAINTY ON THE RESULTS DESCRIBED IN §6.1, §6.3 AND §6.5

Parameter	Nominal Result	MC (variable M)	MC (variable M and SFR)	BP (split)	BP (not split)
n_M	0.67 ± 0.15	0.76 ± 0.07	0.78 ± 0.08	0.68 ± 0.11	0.68 ± 0.11
$n_{\text{star-forming}}$	0.94 ± 0.08	0.93 ± 0.03	0.93 ± 0.04	0.94 ± 0.07	0.94 ± 0.07
$\log A^a$	-9.95 ± 0.68	-10.98 ± 0.73	-11.14 ± 0.82	-10.14 ± 1.13	-10.15 ± 1.12
$\log A^b$	-13.56 ± 0.08	-13.49 ± 0.04	-13.51 ± 0.04	-13.53 ± 0.08	-13.54 ± 0.09
n_{SFR}^a	0.96 ± 0.07	0.96 ± 0.001	0.85 ± 0.10	0.97 ± 0.06	0.97 ± 0.06
n_{SFR}^b	0.98 ± 0.08	0.99 ± 0.001	0.85 ± 0.09	1.00 ± 0.06	1.00 ± 0.06
$\log B^c$	-2.81 ± 0.04	-2.81 ± 0.001	-2.85 ± 0.04	-2.81 ± 0.03	-2.81 ± 0.03
$\log B^d$	-2.81 ± 0.04	-2.83 ± 0.001	-2.90 ± 0.07	-2.82 ± 0.03	-2.82 ± 0.03
$\log B^e$	-2.85 ± 0.04	-2.85 ± 0.001	-2.94 ± 0.09	-2.86 ± 0.02	-2.86 ± 0.02
Passive Rate f	3.6 ± 0.6	3.6 ± 0.01	3.3 ± 0.1	3.6 ± 0.4	3.55 ± 0.4
Starburst Rate f	124.7 ± 29.95	92.2 ± 11.4	85.4 ± 13.8	102.4 ± 18.8	102.8 ± 19.0

^a n_M free, in units of $\text{SNe yr}^{-1} M_{\odot}^{-1}$ ^b $n_M \equiv 1$, in units of $\text{SNe yr}^{-1} M_{\odot}^{-1}$ ^c n_M and n_{SFR} free, $\text{SNe yr}^{-1} (M_{\odot} \text{yr}^{-1})^{-1}$ ^d n_M free and $n_{\text{SFR}} \equiv 1$, $\text{SNe yr}^{-1} (M_{\odot} \text{yr}^{-1})^{-1}$ ^e $n_M \equiv 1$ and $n_{\text{SFR}} \equiv 1$, $\text{SNe yr}^{-1} (M_{\odot} \text{yr}^{-1})^{-1}$ ^f $\times 10^{-14}$ per unit mass per year

forming galaxies. The value of A is consistent with our result ($2.8_{-0.5}^{+0.6} \times 10^{-14} \text{SNe yr}^{-1} M_{\odot}^{-1}$), when $n_M \equiv 1$ is assumed, and our value of $B = 1.4_{-0.1}^{+0.2} \times 10^{-3} \text{SNe yr}^{-1} (M_{\odot} \text{yr}^{-1})^{-1}$ when $n_M \equiv 1$ and $n_{\text{SFR}} \equiv 1$ is also in good agreement. However, as noted, the A+B model for the SN Ia rate that depends linearly on M and \dot{M} does not provide the best-fit for our dataset. Scannapieco & Bildsten (2005); Mannucci et al. (2005) assumed that the SN Ia rate depends linearly on M and \dot{M} . Dilday et al. (2008) using a sample of low redshift SNe ($z < 0.12$) from the SDSS-II SN Survey (and overlapping with this work) combined with other published work, used the global star-formation rate as determined by Hopkins & Beacom (2006) (which may over-estimate the total mass density) to determine $A = (2.8 \pm 1.2) \times 10^{-14} \text{SNe yr}^{-1} M_{\odot}^{-1}$ and $B = (0.93 \pm 0.34) \times 10^{-3} \text{SNe yr}^{-1} (M_{\odot} \text{yr}^{-1})^{-1}$, which are in agreement with those found in this analysis. Li et al. (2010) study how the SN Ia rate is related to the size, color and morphology of the host galaxy for a sample of local SNe. They show that the SN Ia rate is not linearly related to the stellar mass of the host galaxy, instead preferring a relationship, $\text{SNR}_{\text{Ia}} \propto M^{\sim 0.5}$, independent of host galaxy morphology and color. Their result for elliptical galaxies is in excellent agreement with our results for passive galaxies, favor-

ing a SN Ia rate proportional to $M^{0.67 \pm 0.15}$. However, our results differ for star-forming galaxies, where we find that an $\text{SNR}_{\text{Ia}} \propto M^{0.94 \pm 0.08}$ is favored. Li et al. (2010) also consider the case where $\text{SNR}_{\text{Ia}} \propto M$ for elliptical galaxies, finding a value of $A = 4.4_{-0.8}^{+0.9} \times 10^{-14} \text{SNe yr}^{-1} M_{\odot}^{-1}$ (in our framework), which is consistent with our result.

7. SNe Properties

We have studied how the rate of SNe Ia is related to the host galaxy properties and have seen that the rate of SNe is dependent the galaxy stellar mass and star-formation rate. We extend this analysis to consider how the SN Ia light-curve parameters are related to the host galaxy properties. Previously studies by Hamuy et al. (1995, 2000) and Sullivan et al. (2006), for example, found that bright SNe Ia are preferentially seen in young stellar environments, and Hamuy et al. (1996) showed that there is a strong correlation between the light-curve decline rate and the host galaxy morphology. The homogeneity of the SDSS-II SN sample provides an ideal opportunity to determine SN Ia light-curve parameters as a function of the galaxy star-forming rate.

SNe Ia have two key observables that affect their use as cosmological probes; their light-

TABLE 5

A COMPARISON OF THE RESULTS OF §6.1 AND §6.3 FROM THIS PAPER WITH OTHER PUBLISHED ANALYSES.

Analysis	Redshift range covered	n_M^a	n_{SFR}^b	A ^a SNe yr ⁻¹ M _⊙ ⁻¹	B ^b SNe yr ⁻¹ (M _⊙ yr ⁻¹) ⁻¹
This work	0.05 < z < 0.25	0.67 ± 0.15	0.96 ± 0.07	1.11 ^{+4.17} _{-0.88} × 10 ⁻¹⁰	1.55 ^{+0.16} _{-0.15} × 10 ⁻³
This work	0.05 < z < 0.25	fixed = 1	fixed = 1	2.8 ^{+0.6} _{-0.5} × 10 ⁻¹⁴	1.4 ^{+0.2} _{-0.1} × 10 ⁻³
Sullivan et al. (2006)	0.2 < z < 0.75	1.10 ± 0.12	0.84 ± 0.06	-	-
Sullivan et al. (2006)	0.2 < z < 0.75	fixed = 1	fixed = 1	5.3 ± 1.1 × 10 ⁻¹⁴	3.9 ± 0.7 × 10 ⁻⁴
Mannucci et al. (2005) ^{c,d}	low redshift	fixed = 1	fixed = 1	3.83 ^{+1.4} _{-1.2} × 10 ⁻¹⁴	2.3 ± 1. × 10 ⁻³
Dilday et al. (2008) ^e	z < 0.12	fixed = 1	fixed = 1	2.8 ± 1.2 × 10 ⁻¹⁴	0.93 ± 0.34 × 10 ⁻³
Li et al. (2010) ^f	z < 0.05	fixed = 1	-	4.4 ^{+0.9} _{-0.8} × 10 ⁻¹⁴	-

^aAs derived in §6.1

^bAs determined in §6.3

^cResults taken from Mannucci et. al. (2005) and Scannapieco & Bildsten (2005)

^dApproximating E/S0 galaxies for passive galaxies to determine the value of A and using the rate of SNe Ia in blue (B - K) galaxies to determine the value of B

^eUsing the global star-formation rate as determined by Hopkins & Beacom (2006)

^fConsidering Elliptical galaxies as passive galaxies

curve decline rate / peak brightness relationship (Phillips 1993) and their color. In MLCS2k2, the relationship between the peak luminosity of a SN Ia and the shape of its light-curve, is parameterized through the Δ parameter, where smaller Δ values correspond to brighter SNe Ia. The observed color excess of SNe Ia is modelled as the level of extinction in the V band, through the parameter A_V .

7.1. MLCS2k2 Δ Parameter as a Function of Host Galaxy Type

Figure 6 shows the distribution of the MLCS2k2 Δ parameter for the SNe Ia found in passive and star-forming host galaxies (shown both separately and as a combined dataset), after correcting for efficiency as described in §3.2 and §4.4. For the passive galaxies, we find a mean value of $\Delta = 0.20$, with variance 0.14, compared to the star-forming galaxies, which have lower mean value $\Delta = -0.08$ and a smaller variance of 0.06.

A Kolmogorv-Smirnov test (KS test; Chakravarti et al. 1967) and an Anderson-Darling test (AD test; Stephens 1974) are used to test the hypothesis that the two histograms shown in Figure 6 are drawn from the same parent distribution. We find probabilities of 2.67×10^{-13} for the KS test and 3.21×10^{-13} for the AD-test and conclude

that the histograms arise from two different populations. Our result confirms previous findings (Sullivan et al. 2006; Lampeitl et al. 2010b) that SNe in star-forming galaxies are brighter than their passive counter-parts and that SNe in passive galaxies exhibit a broader range of Δ values when compared to their star-forming counterparts.

To investigate further, we split the star-forming galaxy sample into moderately and highly star-forming datasets (as described in §5). When we compare the distribution of Δ in passive galaxies to that of moderately and highly star-forming galaxies, respectively, we find KS test probabilities of 4.8×10^{-9} for moderately star-forming, and 2.9×10^{-13} for highly star-forming galaxies, with comparable values for the AD test. This shows that SNe Ia in star-forming galaxies differ from their passive counterparts, even for moderate levels star-formation. We find a KS test probability of 0.04 (with AD test value 0.004) that the Δ distributions in moderately and highly star-forming galaxies arise from the same parent distribution.

These results are not surprising in the context of a two component model since we have shown that most of the rate even in moderately star-forming galaxies can be attributed to recent star-formation. However, if there were more than two components, or some evolution depending on the

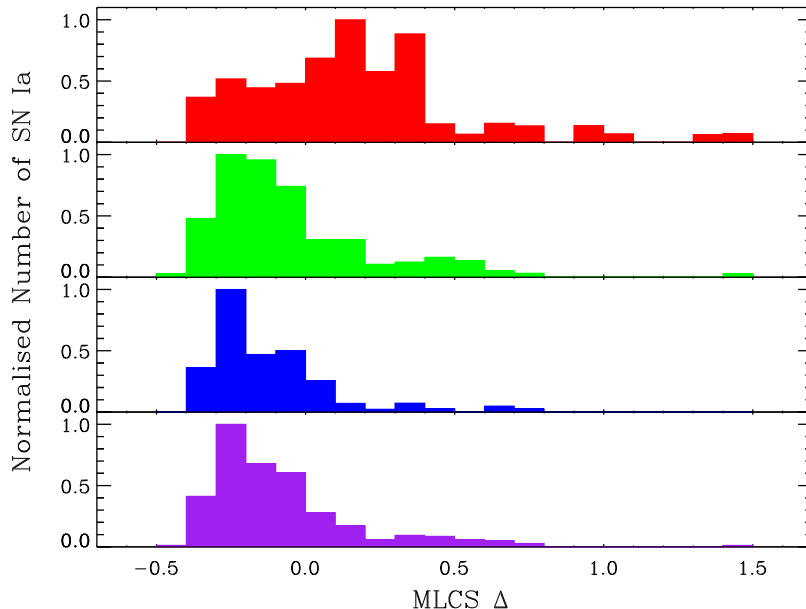


Fig. 6.— The distribution of Δ for SNe found in passive galaxies (*top panel*) is compared to those found in star-forming galaxies. The distributions for moderately star-forming and highly star-forming galaxies are plotted in the second and third panels respectively. (*bottom panel:*) Star-forming galaxies are plotted as a cumulative histogram, with the distributions for moderately star-forming and highly star-forming galaxies combined.

star-forming rate, we might have observed a significant difference between the high star-forming and moderately star-forming distributions.

7.2. MLCS2k2 A_V Parameter as a Function of Host Galaxy Type

Determining the color of SNe Ia is important for cosmological parameter estimation. Recently, Sullivan et al. (2010); Kelly et al. (2010) and Lampeitl et al. (2010b) found evidence that SNe in different environments may follow different color laws. Here we consider how the distribution of color, expressed by the MLCS2k2 A_V parameter, varies as a function of host galaxy sSFR. To examine this relationship we apply a flat prior in MLCS2k2, allowing A_V to take all values (both positive and negative), so that we are not sensitive to assumptions about the distribution of A_V values. The use of a flat prior changes the number of SNe Ia that pass our selection criteria from 342 to 338. The effect of our choice of prior is discussed further in §7.3.

Figure 7 shows the distribution of A_V for SNe in passive hosts and star-forming galaxies. The distributions for moderately star-forming and highly star-forming galaxies are plotted separately, along with the case where the two star-forming datasets have been combined. We use the efficiency correction described in §3.2 and the $1/V_{\max}$ correction determined in §4.4 to weight each galaxy. Passive galaxies have a mean A_V of 0.40mag and variance 0.27, compared to a mean of 0.33mag and variance 0.15 for star-forming galaxies. For the individual star-forming galaxy populations, we find means of 0.43 and 0.22mag and variances of 0.16 and 0.12 for moderately and highly star-forming galaxies, respectively.

As in §7.1 we use both KS and AD tests to indicate whether the distributions are drawn from the same parent distributions. We find probabilities of 0.163 and 0.049 respectively, suggesting no evidence that the distributions may be drawn from different parent distributions. These results are consistent with Lampeitl et al. (2010b), who used

the SDSS spectroscopically confirmed SNe fitted with the SALT2 light-curve fitter, and saw no significant difference in the distribution of the SALT2 color parameter, c , for SNe Ia’s in passive and star-forming galaxies.

As before, we split the star-forming dataset in to moderately and highly star-forming galaxies. We fit KS test probabilities of 0.42 when passive and moderately star-forming datasets are considered, 8.0×10^{-4} for passive and highly star-forming, and 2.3×10^{-4} between the two star-forming datasets, and comparable AD test statistics. We conclude that whilst there is no evidence of a difference in the A_V distributions between the passive and moderately star-forming datasets, the highly star-forming sample has a different distribution in A_V , as shown in Figure 7, with SNe Ia in highly star-forming galaxies on average exhibiting smaller values of A_V .

This analysis assumes that the observed values of A_V are good approximations to the true underlying values. However, while the majority of SNe in our sample have well measured light-curves, resulting in accurate measurements of A_V , many of the SNe Ia in our sample have low S/N measurements. In such cases, since the underlying distribution of A_V for SNe Ia is observed to be exponentially declining, the measured value of A_V , for an individual SNe, is more likely to be scattered towards a higher value of A_V than a lower value. This would result in a higher proportion of SNe with high A_V measurements compared to a distribution of SNe Ia with high S/N light-curves.

To rigorously account for S/N variations in the observations, the underlying Δ and A_V distributions are determined using the method described in D’Agostini (1995) and Appendix D of Kessler et al. (2009a). To quantify the uncertainty in the underlying distributions, 60 data-sized simulations were analyzed in the same way as the data. The spread in the mean and RMS of the extracted distributions are taken to be the uncertainties in these quantities. To avoid pathologies from poorly measured photometric redshifts, only SNe Ia with a spectroscopic redshift (either from the SNe or host galaxy) are used. The resulting incompleteness was modelled in simulations and found to have a negligible impact on the results. Based on the spread in the distribution moments (both mean and RMS), we estimate that the distribu-

tion of A_V in highly star-forming galaxies differs from that of passive and moderately star-forming galaxies at 3.3σ and 3.5σ , respectively.

For our sample, SNe Ia have similar S/N values at maximum brightness, for all host galaxy types. SNe Ia in passive galaxies have a mean S/N of 36 (with RMS of 26) compared to means of 33 and 42 and variances of 17 and 30 for SNe Ia in moderately star-forming and highly star-forming galaxies, respectively.

Finally, we use the SALT2 light-curve fitter (Guy et al. 2007, 2010) to determine if our results are dependent on light-curve fitting technique. SALT2 uses a color term, c , as a measure of the color of an individual SN Ia, but does not explicitly attribute it to dust extinction. We recover the underlying distribution of c for SNe in our sample, following the technique of D’Agostini (1995), and find that the both the mean and RMS of the color distribution for SNe Ia in highly star-forming galaxies is different from those in passive and moderately star-forming galaxies at 2.7σ and 3.8σ , respectively.

A physical understanding of this difference is unclear. Sargsyan et al. (2010) suggest that there may be an increased amount of dust observed in star-burst galaxies, whilst Salim et al. (2005) argue that the dust content is smaller, and covers a smaller range, in low mass, highly star-forming galaxies.

The similarity between passive and moderately star-forming galaxies suggests that much of the spread in color could arise from variations in the explosion process or effects of the local SN environment (Maeda et al. 2011). If host galaxy dust were responsible for the difference we would expect to see less extinction in passive galaxies since they have lower dust levels (Calzetti 1998).

7.3. The Effect of our Selection Criteria

In §6.6 we considered how the inclusion of non-spectroscopically confirmed SNe Ia and our redshift range affected the results of §6.1, §6.3 and §6.5. Here, we carry out a similar analysis on the results of §7.1 and §7.2. We also consider how the A_V prior used in the MLCS2k2 light-curve fits affect our conclusions.

Tables 6 and 7 show the KS test probabilities described in §7.1 and §7.2 for various selection cri-

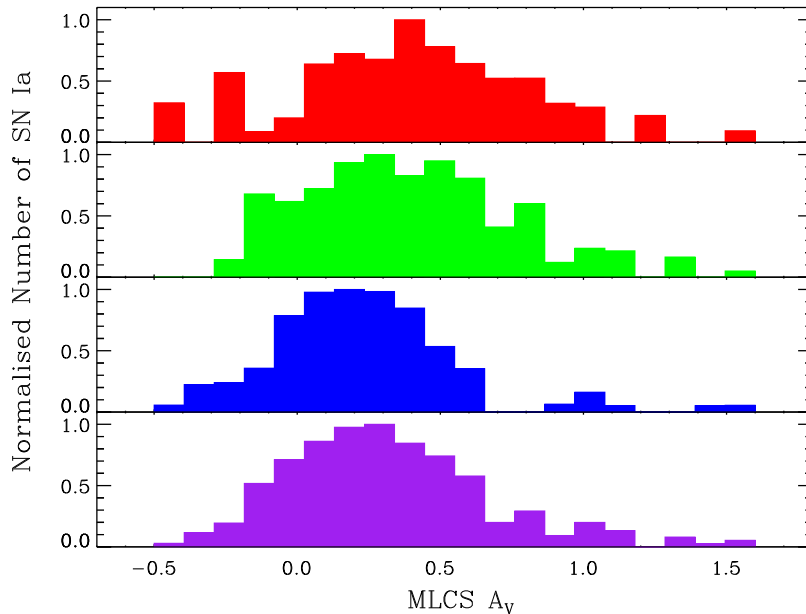


Fig. 7.— The distribution of A_V for SNe found in passive galaxies (*top panel*) is compared to those found in star-forming galaxies. The distributions for moderately star-forming and highly star-forming galaxies are plotted in the second and third panels respectively. The bottom panel is the sum of the two middle panels, showing the combined distribution for star-forming galaxies. A flat prior is used in the light-curve fitting.

teria. We consider the “standard” A_V prior discussed in §3.1, a flat A_V prior, as used in §7.2 and a prior where A_V is forced to positive. We also consider the effect of varying our redshift range, and considering only spectroscopically confirmed SNe Ia.

From Table 6 we see that in all cases considered, there is a very low probability that the distribution of Δ from SNe in passive galaxies matches that seen in star-forming galaxies. Similarly, the evidence that highly and moderately star-forming galaxies are different is consistently weak. Table 7, shows the KS test probabilities for the A_V distributions. As in §7.2, there is no evidence that the distribution of A_V in passive galaxies differs from that seen in star-forming galaxies. There is evidence that the distribution of A_V in highly star-forming galaxies does not match that of passive and moderately star-forming galaxies.

From Figure 6, we observe that fainter, higher Δ , SNe are preferentially found in passive galaxies. However, the survey efficiency considered for this analysis, is a function of redshift, and does not

distinguish between SNe Ia of differing intrinsic brightness. To account for this, we consider how modelling the survey efficiency as a function of both A_V and Δ affects our conclusions, and find that our results are unaffected by this additional correction.

In §7.2, we used the SALT2 light-curve fitter to show that our results concerning the distribution of A_V (or c) for SNe Ia as a function of host galaxy type are independent of light-curve fitting technique considered. SALT2 parameterizes the relationship between the peak luminosity of a SN Ia and the shape of its light-curve through the x_1 parameter. We recover the underlying distribution of x_1 for SNe in our sample, and find that both the mean and RMS of the x_1 distribution for SNe Ia in passive galaxies differs from those found in moderately and highly star-forming galaxies at 4.6σ and 9.6σ , respectively, confirming the results of §7.1.

We further considered the possibility that our results may depend on survey conditions or may vary as a function of position on the sky. We split

the host galaxy sample by both year and position but saw no significant effects.

8. Conclusions

We have studied how the SN Ia rate and light-curve properties depend on the host galaxy stellar mass and star-formation rate. By augmenting the SDSS spectroscopically confirmed SNe Ia with SNe identified by only their light-curves, we have constructed a large, homogeneous and well-understood sample of 342 SNe Ia in the redshift range $0.05 < z < 0.25$. Our sample has low contamination and is unbiased with respect to spectroscopic selection effects and survey conditions. The efficiency of the SDSS-II SN Survey is well measured in this redshift range, allowing us to study the overall SN Ia rate as a function of these host galaxy properties. We summarize below the main conclusions of this work:

- We find that the SN Ia rate in passive galaxies is not linearly proportional to the stellar mass, but instead favoring $\text{SNR}_{\text{Ia}} \propto M^{0.67}$, as illustrated in Figure 3. This result differs from that of Sullivan et al. (2006), at higher redshift, who favor a linear relationship, but is in good agreement with the conclusions of Li et al. (2010), who favor $\text{SNR}_{\text{Ia}} \propto M^{0.487 \pm 0.316}$ for elliptical galaxies in the local Universe.
- For star-forming galaxies we find that the SN Ia rate as a function stellar mass differs from that of passive galaxies, instead favoring $\text{SNR}_{\text{Ia}} \propto M^{0.94}$. This result differs from that of Li et al. (2010), who found that the SN Ia rate as a function of stellar mass is independent of host galaxy morphology and color.
- We show that the SN Ia rate per unit stellar mass is a strong function of specific star-formation rate (sSFR), with SNe Ia being preferentially found in highly star-forming or starburst galaxies, compared to their passive counterparts (Figure 5). This relationship is consistent with those found by Mannucci et al. (2005) and Sullivan et al. (2006), locally and at high redshift, respectively, implying that this relationship does not evolve with redshift.
- We demonstrate that the excess SN Ia rate in star-forming galaxies is well fit by a linear relationship proportional to the recent star-formation rate, as shown in Figure 4. The component related to recent star-formation is the dominant contributor to the SN Ia rate in these galaxies.
- We find that a bivariate fitting technique confirms that SNe Ia in this sample satisfy a SN Ia rate of the form $\text{SNR}_{\text{Ia}} = 1.1 \pm 0.2 \times 10^{-10} M^{0.7 \pm 0.01} + 1.0 \pm 0.1 \times 10^{-3} \dot{M}^{1.0 \pm 0.1}$ (statistical errors only). This parameterization is a generalization of the A+B model and provides a better fit to the SDSS-II SN data than assuming a SN Ia rate linearly dependent on stellar mass and star-formation rate.
- We have tested the effect of our selection criteria on these results, and find that the exclusion of photometrically classified SNe Ia's, and variations in redshift range, do not significantly alter our results.
- We confirm the striking difference in light-curve shape between passive and star-forming galaxies. Specifically, brighter, slowly declining SNe (with smaller Δ values for MLCS2k2) are seen preferentially in star-forming galaxies while faint, quickly declining SNe (with high Δ values) are preferentially found in passive galaxies as shown in Figure 6.
- We see no difference in the distribution of the extinction parameter, A_V , between passive and star-forming galaxies as illustrated in Figure 7. We find no evidence that the distribution of A_V in passive galaxies differs from that of moderately star-forming galaxies, but find evidence that the distribution is different for highly star-forming galaxies, which favor lower mean values of A_V . We use the method described in Appendix D of Kessler et al. (2009a) to determine the underlying distribution of A_V for various galaxy types, and show that the distribution of A_V in highly star-forming galaxies differs at the 3σ level from that of passive and moderately star-forming galaxies. We find that the choice of A_V prior used in the

TABLE 6

EFFECT OF OUR SELECTION CRITERIA ON THE RESULTS DESCRIBED IN §7 ON THE DISTRIBUTION OF THE LIGHT-CURVE DECLINE RATE PARAMETER, Δ

Selection	No. Hosts	KS-test for Δ distribution	
		Passive / Star-forming	High / Mod.
Std A_V Prior	342	2.67×10^{-13}	0.037
Flat A_V Prior	338	6.37×10^{-12}	0.040
Positive A_V Prior	364	3.66×10^{-14}	0.037
Confirmed	197	2.31×10^{-12}	0.020
Phot-ID	145	2.17×10^{-3}	0.137
$z < 0.20$	196	8.79×10^{-8}	0.070
$z < 0.16$	103	3.00×10^{-5}	0.295

TABLE 7

EFFECT OF OUR SELECTION CRITERIA ON THE RESULTS DESCRIBED IN §7 ON THE DISTRIBUTION OF A_V

Selection	No. Hosts	KS-test for A_V distribution			
		Passive / Star-forming	Passive / Mod.	Passive / Highs	Mod. / Highs
Std A_V Prior	342	0.295	0.889	6.11×10^{-3}	1.10×10^{-4}
Flat A_V Prior	338	0.163	0.416	7.98×10^{-4}	2.31×10^{-4}
Positive A_V Prior	364	0.036	0.923	3.07×10^{-4}	1.13×10^{-4}
Confirmed	197	0.320	0.843	0.022	3.13×10^{-3}
Phot-ID	145	0.573	0.390	0.271	0.018
$z < 0.20$	196	0.542	0.606	0.034	1.00×10^{-4}
$z < 0.16$	103	0.612	0.032	0.240	8.04×10^{-5}

light-curve fitting does not affect our conclusions. We find the same results using the SALT2 model to extract the distribution of color, c , thus providing evidence that the difference in the distribution of A_V (or c) is a model-independent feature.

- We perform a rigorous test of the PÉGASE.2 SEDs and the Z-PEG fitting technique and find a systematic offset in the photometric redshift estimates produced for our comparison field sample. If a simple correction is applied to both the redshifts and stellar masses of our field sample, we find that our conclusions are unchanged.

The process used to determine our sample of host galaxies and their derived properties allows us to directly compare our conclusions with those of Sullivan et al. (2006), who studied the SN Ia rate at higher redshifts. Sullivan et al. (2006) found the same trends with star-formation rate, but with a different relationship parameterizing the stellar mass into the SN Ia rate. It is unlikely that these differences are due to an evolution of the galaxy

population but may reflect that SNe Ia are primarily triggered by recent bursts of star-formation in a galaxy, causing uncertainties in the contribution due to the stellar mass.

Acknowledgements

The authors thank Mark Sullivan, Damien Le Borgne, Claudia Maraston and Janine Pforr for helpful discussions. MS is funded by an SKA fellowship, while RCN and HL are supported by STFC. MS thanks Prina Patel and Russell Johnston for insightful comments. Support for this research at Rutgers University was provided in part by NSF CAREER award AST-0847157 to SWJ.

Funding for the SDSS and SDSS-II has been provided by the Alfred P. Sloan Foundation, the Participating Institutions, the National Science Foundation, the U.S. Department of Energy, the National Aeronautics and Space Administration, the Japanese Monbukagakusho, the Max Planck Society, and the Higher Education Funding Council for England. The SDSS Web Site is <http://www.sdss.org/>.

The SDSS is managed by the Astrophysical Research Consortium for the Participating Institutions. The Participating Institutions are the American Museum of Natural History, Astrophysical Institute Potsdam, University of Basel, University of Cambridge, Case Western Reserve University, University of Chicago, Drexel University, Fermilab, the Institute for Advanced Study, the Japan Participation Group, Johns Hopkins University, the Joint Institute for Nuclear Astrophysics, the Kavli Institute for Particle Astrophysics and Cosmology, the Korean Scientist Group, the Chinese Academy of Sciences (LAMOST), Los Alamos National Laboratory, the Max-Planck-Institute for Astronomy (MPIA), the Max-Planck-Institute for Astrophysics (MPA), New Mexico State University, Ohio State University, University of Pittsburgh, University of Portsmouth, Princeton University, the United States Naval Observatory, and the University of Washington.

This work is based in part on observations made at the following telescopes. The Hobby-Eberly Telescope (HET) is a joint project of the University of Texas at Austin, the Pennsylvania State University, Stanford University, Ludwig-Maximilians-Universität München, and Georg-August-Universität Göttingen. The HET is named in honor of its principal benefactors, William P. Hobby and Robert E. Eberly. The Marcario Low-Resolution Spectrograph is named for Mike Marcario of High Lonesome Optics, who fabricated several optical elements for the instrument but died before its completion; it is a joint project of the Hobby-Eberly Telescope partnership and the Instituto de Astronomía de la Universidad Nacional Autónoma de México. The Apache Point Observatory 3.5 m telescope is owned and operated by the Astrophysical Research Consortium. We thank the observatory director, Suzanne Hawley, and site manager, Bruce Gillespie, for their support of this project. The Subaru Telescope is operated by the National Astronomical Observatory of Japan. The William Herschel Telescope is operated by the Isaac Newton Group, on the island of La Palma in the Spanish Observatorio del Roque de los Muchachos of the Instituto de Astrofísica de Canarias. Based on observations made with the Nordic Optical Telescope, operated on the island of La Palma jointly by Den-

mark, Finland, Iceland, Norway, and Sweden, in the Spanish Observatorio del Roque de los Muchachos of the Instituto de Astrofísica de Canarias. Kitt Peak National Observatory, National Optical Astronomy Observatory, is operated by the Association of Universities for Research in Astronomy, Inc. (AURA) under cooperative agreement with the National Science Foundation. The W.M. Keck Observatory is operated as a scientific partnership among the California Institute of Technology, the University of California, and the National Aeronautics and Space Administration. The Observatory was made possible by the generous financial support of the W. M. Keck Foundation. Based partially on observations made with the Italian Telescopio Nazionale Galileo (TNG) operated on the island of La Palma by the Fundación Galileo Galilei of the INAF (Istituto Nazionale di Astrofisica) at the Spanish Observatorio del Roque de los Muchachos of the Instituto de Astrofísica de Canarias.

A. Color-Magnitude Diagram

In §5 we considered how our host galaxies are distributed as a function of stellar mass and star-formation rate, and noted the presence of a subset of galaxies with low-levels of specific star-formation rate. These galaxies do not exhibit high χ^2 values. Figure 8 shows the color-magnitude diagram for the host galaxies used in this analysis. The sample is split into passive, moderately and highly star-forming as described in the caption for Figure 2. The subset of 55 galaxies with low levels of sSFR ($-11.0 < \text{sSFR} < 10.5$) are plotted as light-green triangles. We see that the PÉGASE.2 SED primarily determine the level of star-formation activity in a galaxy based on its color, with passive galaxies being the “reddest” and brightest galaxies through to the “bluest” galaxies being classified as highly star-forming. From Figure 8, the population of objects with low sSFR but classified as moderately star-forming are observed to lie between the passive and the other moderately star-forming galaxies in color-magnitude space, making their classification understandable, if ambiguous. Figure 8 uses absolute magnitudes and colors, but the same conclusions can be drawn when apparent magnitudes are considered. We note that, 43 of the 55 (78%) “ridge line” galaxies are best described by the lenticular (S0) scenario, with the remaining 12 being best-fit by the elliptical galaxy template, possibly highlighting the uncertainty in the nature of lenticular galaxies. In comparison, only 41 of the 79 (52%) remaining moderately star-forming galaxies are best-fit by an S0 template.

To further investigate the nature of the “ridge-line” galaxies, we study the how distribution of Δ for SNe in these galaxies compare to those in moderately star-forming and passive galaxies, since, as described in §7.2, there is a significant difference in the Δ distributions for SN Ia occurring in these galaxies. A K-S test between the distribution of Δ in passive galaxies to that of “ridge-line galaxies” yields a probability of 1.9×10^{-5} that they are drawn from the same parent distribution. This compares to a probability of 0.28 between the distribution of Δ in “ridge-line” galaxies and other moderately star-forming galaxies. These results, further strengthen the conclusion that the “ridge-line” galaxies are not misclassified passive galaxies.

We thus determine that this population of objects is well defined according to color-magnitude space, and that the PÉGASE.2 SEDs use this information to determine the level of star-formation activity in each host galaxy.

B. The PÉGASE.2 Photometric Redshifts

One of the key systematic uncertainties in this analysis concerns the accuracy of the derived properties of the comparison field sample used, and in particular the photometric redshift estimates produced by the PÉGASE.2 SEDs. These redshift estimates will affect not only the number of field galaxies, but also their associated stellar masses. The photometric redshift estimates have been tested at high redshift by Sullivan et al. (2006), but have not been extensively used in the local Universe.

To test the accuracy of the photometric redshifts, we use the host galaxy sample described in §4, and whose properties are listed in Table 9. This sample covers the magnitude range of the comparison field sample and is large enough to statistically determine if the photometric estimates are accurate. Figure 9 shows the difference between the photometric redshift estimates and the known spectroscopic redshift for this sample as a function of both redshift and apparent magnitude. We find a mean difference of 0.03 in redshift, with the photometric redshifts being smaller than the spectroscopic redshift. From Figure 9, there is no evidence of this offset being dependent on either the redshift or apparent magnitude of the host galaxy, although the scatter does increase with apparent magnitude.

This observed offset in the photometric redshift will also lead to an incorrect value for the galaxy’s stellar mass. To quantify this, we consider the derived stellar mass when the redshift is held fixed, compared to that when it is allowed to float in Figure 10, resulting in the offset described above. An offset of $\log M = 0.22$ is seen, with the stellar masses derived when the redshift is allowed to float being smaller than the value determined when the redshift is known.

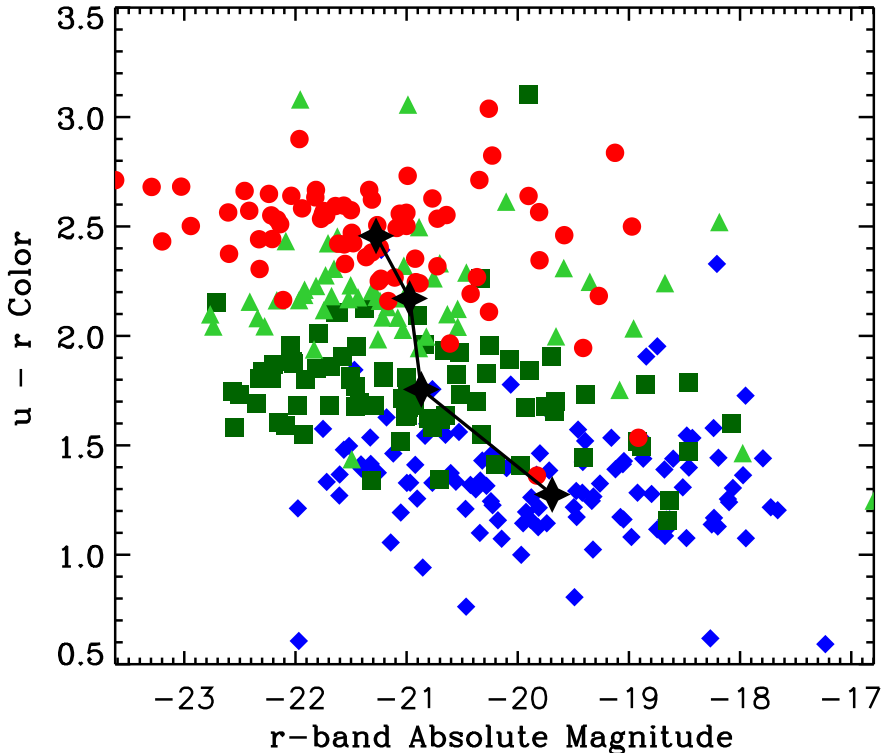


Fig. 8.— Color ($u-r$) versus absolute magnitude for the host galaxy sample used in this analysis. Galaxies classified as passive are plotted as red circles, with highly star-forming galaxies shown as blue diamonds. Moderately star-forming galaxies are plotted in green, with light-green triangles indicating the “ridge-line” of galaxies discussed in §5 and shown in Figure 2. The mean of each individual distribution is shown as a black star, to indicate the relationship between color and brightness for the various samples.

C. The Effect of the Observed Offset on the Conclusions of this Work

The offset between the photometric redshifts produced by the PÉGASE.2 SEDs and the spectroscopic redshifts for the host galaxy sample implies that the distribution of galaxies in the comparison field sample used in this analysis do not accurately reflect the distribution of galaxies in our redshift range. This may affect the results of §6. Here we attempt to quantify this systematic uncertainty.

In Appendix A, we observed that there is a strong dependence between the color of the host galaxy and the best-fitting PÉGASE.2 template determined by the Z-PEG code. This is true for colors determined both by using absolute and apparent magnitudes. The reddest galaxies (in $u-r$) are well-fit by a passive template, through to the bluest galaxies, which are considered to be highly star-forming. Thus, it appears that, we can approximately describe the level of star-formation inferred by the PÉGASE.2 templates as purely a function of observed quantities, and not affected by the offset described in Appendix B. We hence assume, for this analysis, that the offset in the photometric redshifts determined from the PÉGASE.2 SEDs in our redshift range purely affect the inferred stellar masses and not the star-formation rates. We note that this approximation will only be valid for galaxies spanning a narrow redshift range, as large relative k-correction terms can lead to a color dependence, affecting the relationship determined in Figure 8.

In Appendix B we showed that there is no evidence that the difference in redshift ($|z_{\text{photo}} - z_{\text{spec}}|$)

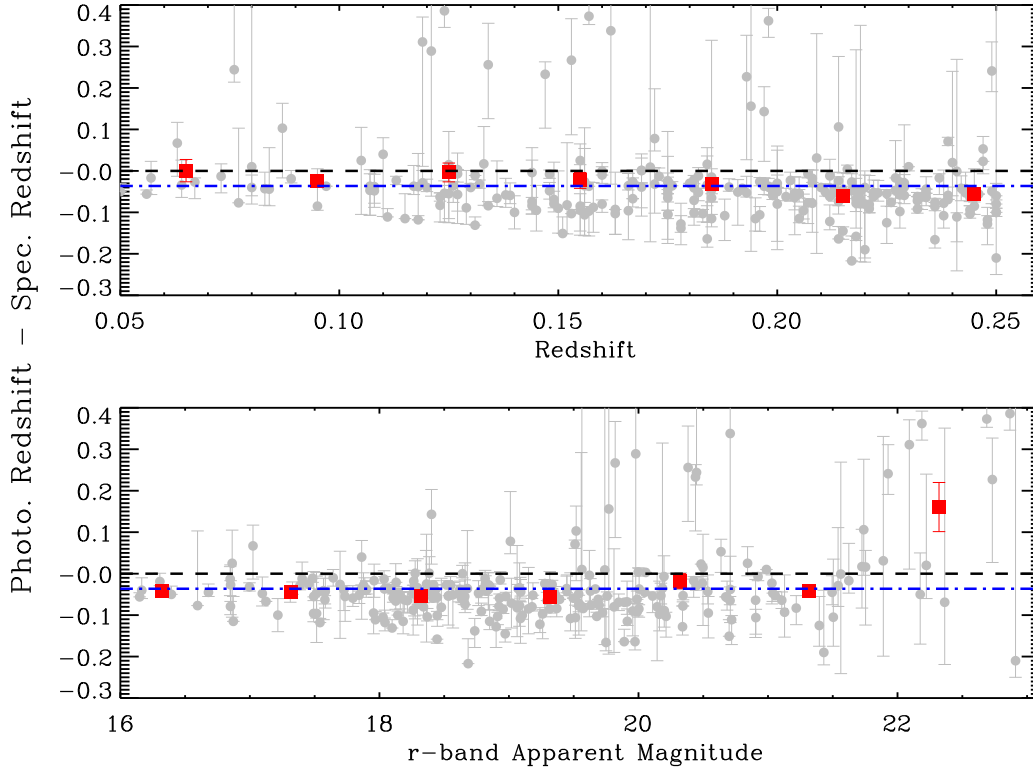


Fig. 9.— *Top*: The difference between the photometric redshift estimates derived from the PÉGASE.2 SEDs and the spectroscopic redshift as a function of redshift. *Bottom*: Same as above, as a function of host galaxy apparent magnitude. Individual galaxies are plotted in grey, with red points indicating the values determined when the sample has been binned. The black, dashed line indicates no difference, while the blue (dashed-dotted) line indicates the mean difference.

and difference in stellar mass ($|\log M(z_{\text{photo}}) - \log M(z_{\text{spec}})|$) are dependent on either redshift or apparent magnitude. We thus assume that the photometric redshifts derived from the PÉGASE.2 SEDs and associated stellar masses can be offset by the values determined in Appendix B. Table 8 shows the effect that correcting the redshifts and stellar masses of the comparison field sample has on several of the key parameters discussed in this work, when the differences found in Appendix B are applied.

From Table 8, it is clear that the number of field galaxies in the redshift range, $0.05 < z < 0.25$, is dramatically reduced when this corrections is applied, but there is also an increase in stellar mass of each galaxy, resulting in the total stellar mass of the field sample being increased from when no correction is applied. Consequently, the SN Ia rate per unit stellar mass per year in passive galaxies is decreased (at the 2.4σ level, when only statistical errors are considered) when the correction is made. This is still in good agreement with other measurements Sullivan et al. (2006); Mannucci et al. (2005).

When considering the effect that the offset in redshift and stellar mass has on the exponents considered for the SN Ia rate, we see that the value of the slope determined in §6.1 decreases, although only by 1.6σ .

TABLE 8

TABLE SHOWING HOW THE SN RATE PARAMETERS DETERMINED IN THIS PAPER ARE ALTERED WHEN THE OFFSETS IN REDSHIFT AND STELLAR MASS, AS DETERMINED IN APPENDIX B, ARE APPLIED TO THE COMPARISON FIELD SAMPLE

Parameter	Original Result	Mean Offset
No. Field Galaxies ^a	733688	615906
Total Stellar Mass of Field Galaxies ^{a,b}	6.67	9.50
Passive Rate ^c	3.56 ± 0.45	2.49 ± 0.31
n_M ^d	0.680 ± 0.150	0.445 ± 0.120
n_{SFR} ^e	0.940 ± 0.078	0.782 ± 0.061
n_{SFR} (when $n_M = 1$) ^f	0.987 ± 0.081	1.070 ± 0.075
n_{SFR} (when $n_M \neq 1$) ^g	0.955 ± 0.074	1.041 ± 0.070

^aAfter the magnitude cut ($15.5 < r < 23.0$) and redshift cut ($0.05 < z < 0.25$)

^bIn units of $1 \times 10^{15} M_{\odot}$

^cThe SN rate per unit stellar mass per year in passive galaxies, as described in §6.5, in units of 1×10^{-14} per unit stellar mass per year

^dThe SN rate per galaxy per year for passive galaxies as a function of log stellar mass, as described in §6.1

^eAs *d*, except for all star-forming galaxies combined, as described in §6.1

^fThe SN rate per galaxy per year for star-forming galaxies as a function of log star-formation rate, after assuming a component proportional to the stellar mass, as described in §6.3

^gAs *f*, only assuming a component proportional to the values determined in *d*, as described in §6.3

In both cases, a linear relationship between the SN Ia rate per galaxy per year and stellar mass in passive galaxies is strongly disfavored, confirming the results of §6.1.

There is a corresponding decrease in the relationship between SN Ia rate and stellar mass for star-forming galaxies (at the 2.0σ level), although as in the main result, there is a clear difference between the rate in passive galaxies when compared to that in star-forming galaxies, indicating the need for a SN Ia rate that is dependent on more than stellar mass. Finally, we consider the results of §6.3. These results are statistically unaffected by the offset discovered in Appendix B. We thus conclude that the main results of this work, namely that the SN Ia in passive galaxies is not linearly related to the stellar mass, and that the SN Ia rate in star-forming galaxies is dominated by any recent burst of star-formation, are not dependent on issues surrounding the ability of PÉGASE.2 to accurately determine the photometric redshifts for our comparison field sample. These corrections are not applied in our analysis as a clear understanding of the cause of this offset has not been found, and thus we have only been able to estimate the magnitude of its effect on our results.

D. The PÉGASE.2 Stellar Mass and SFR Estimates

In Appendix B we compared the PÉGASE.2 photometric redshifts to a similarly distributed sample of galaxies with spectroscopic redshifts, and determined a bias in both redshift and stellar mass. Here we consider how our derived properties from the PÉGASE.2 SEDs compare to those determined from the spectral features of a sample of SDSS-I galaxies. Kauffmann et al. (2003) and Brinchmann et al. (2004) used the 4000\AA break and the Balmer absorption line index ($H\delta_A$) to measure the stellar masses and instantaneous star-formation rates for galaxies in the SDSS-I DR4 spectroscopic catalog (Adelman-McCarthy et al. 2006).

While a comparison between the stellar mass and star-formation rates determined by the PÉGASE.2 templates and the results of Kauffmann et al. (2003) and Brinchmann et al. (2004) may have limitations (this sample consists of only the brightest galaxies in our host galaxy sample, the resolution of the SDSS-I spectra is not optimal, and this method relies on the same underlying physics as the PÉGASE.2 templates), it provides a useful validation of the PÉGASE.2 measurements. We use $\sim 330,000$ galaxies from the SDSS-I catalog, limiting ourselves to the redshift range considered in this analysis. Several spectral measurements are available; we use the dust-corrected stellar mass (median value) and total star-formation rate (median of the likelihood distribution), and determine estimates from the PÉGASE.2 SEDs using the spectroscopic redshifts and model magnitudes.

Figure 11 shows the relationship between the spectroscopic and photometric estimates of stellar mass and star-formation rate. The total stellar mass is well recovered, with a mean offset of only $\Delta \log M = 0.001$, and variance 0.028, well below the range significant for our analysis.

No variation is seen with redshift or apparent magnitude. The relationship with star-formation rate shows greater scatter. We find a mean difference of $\log \text{SFR} = 0.115$ and variance 0.216, with estimates from PÉGASE.2 being larger. This is not surprising, primarily as PÉGASE.2 estimates the mean star-formation rate averaged over the last 0.5Gyr, while Brinchmann et al. (2004) attempts to determine the instantaneous star-formation rate.

Nevertheless, the PÉGASE.2 and Brinchmann et al. (2004) values agree to within 30% while the star-forming rates span over two orders of magnitude. No variation is seen as a function of redshift or apparent magnitude. We note that this analysis has primarily considered passive and star-forming galaxies separately, which does not require an accurate measurement of the star-forming rate.

E. Rest Wavelength Coverage

Throughout this analysis we have compared our observations at $z < 0.25$ to those at higher redshift (Sullivan et al. 2006). While our methodology is identical to that used by Sullivan et al. (2006), both

analyses use filter sets that cover the same observed wavelength range, and thus the PÉGASE.2 SED fits are carried out over different rest-wavelength ranges. To test how this difference may affect our conclusions, specifically the comparison to Sullivan et al. (2006), we consider how carrying out our PÉGASE.2 fits using a reduced number of filters affects the derived stellar mass and star-formation rates.

The analysis of Sullivan et al. (2006) covers a bluer part of the rest-wavelength spectrum than our analysis. Thus, to produce a combination of filters that closely mimics their work, we use a reduced number of filters, removing the reddest bands from the fitting process. Specifically we investigate the cases where only the *ugr* and *ugri* filters are used.

Figures 12 and 13 show the difference, as a function of apparent magnitude, between the stellar masses and star-formation rates derived by the PÉGASE.2 SEDs when various filter combinations are used. As the number of filters is reduced, and thus the number of data points used in the PÉGASE.2 fits is reduced, the scatter between the stellar mass and star-formation rate distribution is increased. However, in the case where 4 filters are considered, no significant offset is seen, with a mean difference of $\log M = -0.02$, where galaxies are determined to be slightly less massive when only four filters are used. The star-formation rates are well recovered, with a mean difference of $\log \text{SFR} = -0.024$, and scatter $\sigma = 0.141$. There is no evidence that this result is dependent on the magnitude of the galaxy. Altering the number of filters used in the PÉGASE.2 fits allows each galaxy to be classified differently. Of the 85 galaxies that were considered passive when five filters are used, only three (3.6%) are classified as star-forming, when the *z*-band is omitted.

When only three filters are used to determine the derived parameters, the observed scatter increases as expected for both the stellar mass and star-formation rate distributions. A mean difference of $\log M = -0.12$ with scatter $\sigma = 0.23$ is seen. For the star-formation rate distribution, a scatter with mean difference $\log \text{SFR} = -0.12$ and $\sigma = 0.23$ is found. ten galaxies (11.8%) that were considered to be passive when all five filters were considered are classified as star-forming when only the *ugr* filters are used in the PÉGASE.2 fits. Four galaxies (1.5%) which were previously classified as star-forming are determined to be passive when only three filters are used. No trend with apparent magnitude is evident in either case.

Since the extra information from the *i* and *z* filters does not seem to significantly cause an offset in the PÉGASE.2 fits to higher or lower stellar masses or star-formation rates, it appears that the rest-wavelength coverage does not affect our comparisons to Sullivan et al. (2006).

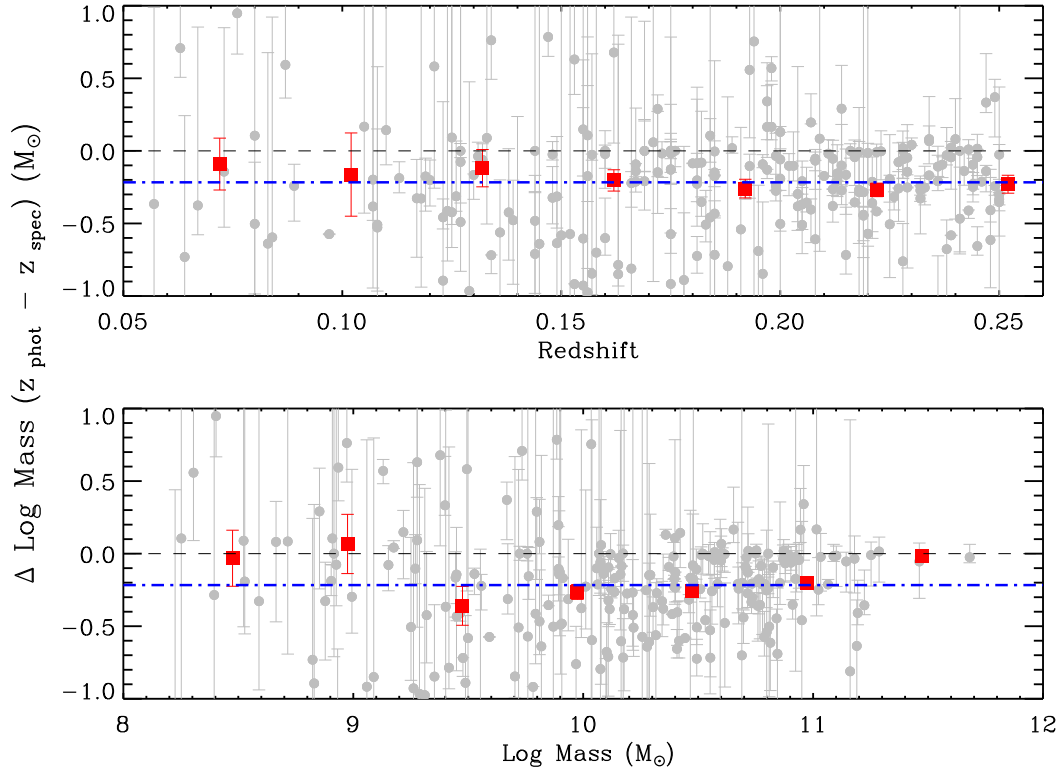


Fig. 10.— *Top*: The difference between the stellar mass derived when the redshift is allowed to float in the Z-PEG code compared to that when the redshift is held fixed, resulting in the offset described in Figure 9, as a function of redshift. *Bottom*: Same as above, as a function of stellar mass, as derived when the redshift is held fixed. Individual galaxies are plotted in grey, with red points indicating the values determined when the sample has been binned. The black, dashed line indicates no difference, while the blue (dashed-dotted) line indicates the mean difference.

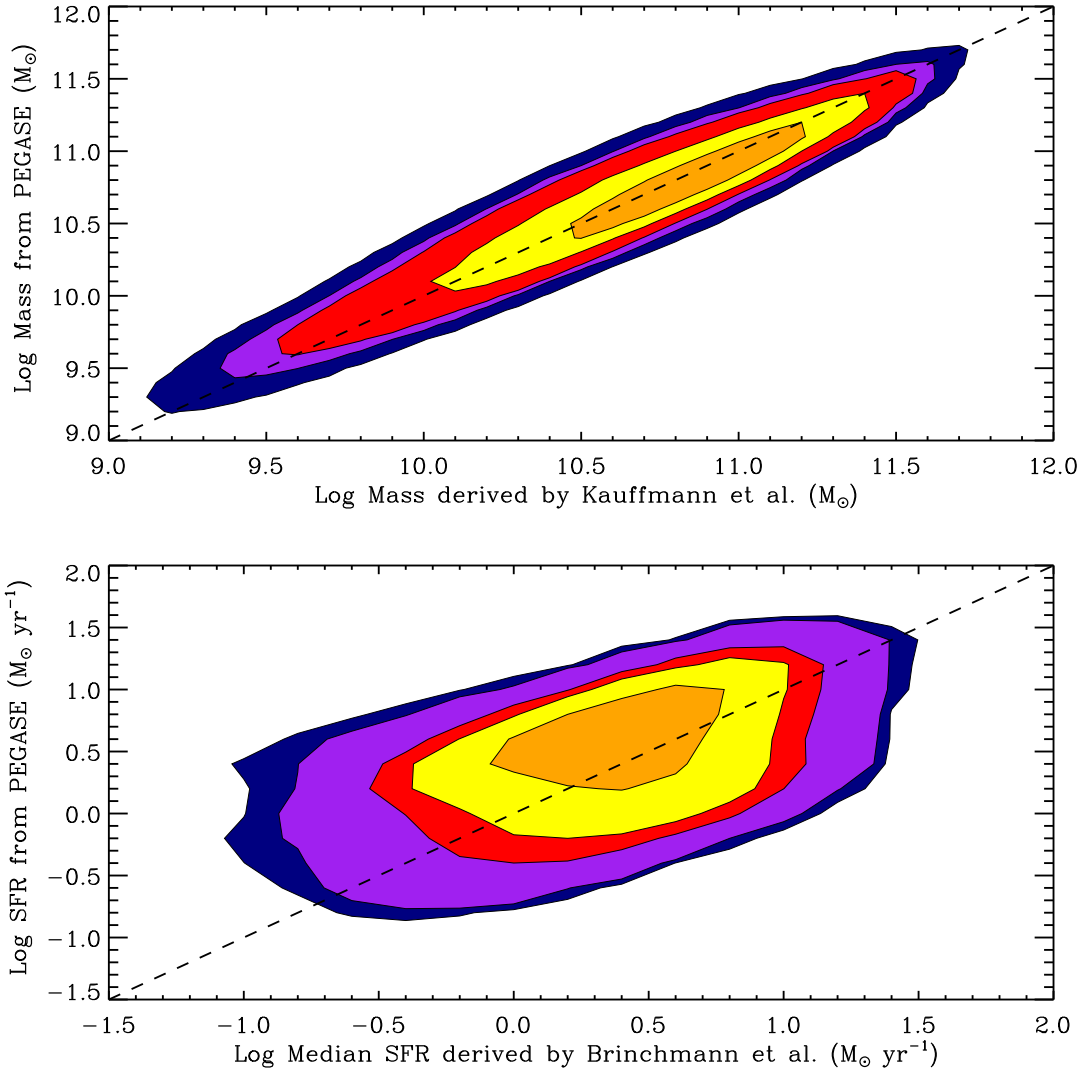


Fig. 11.— *Top*: Log stellar mass derived from the PÉGASE.2 templates for a sample of $\sim 330,000$ galaxies from SDSS-I, compared to the estimates obtained from spectral features by Kauffmann et al. (2003) *Bottom*: Same as above, comparing PÉGASE.2 star-formation rates to those of Brinchmann et al. (2004). Contours enclose 99% (dark blue), 95% (purple), 90% (red) 68% (yellow) and 35% (orange) of the data, respectively.

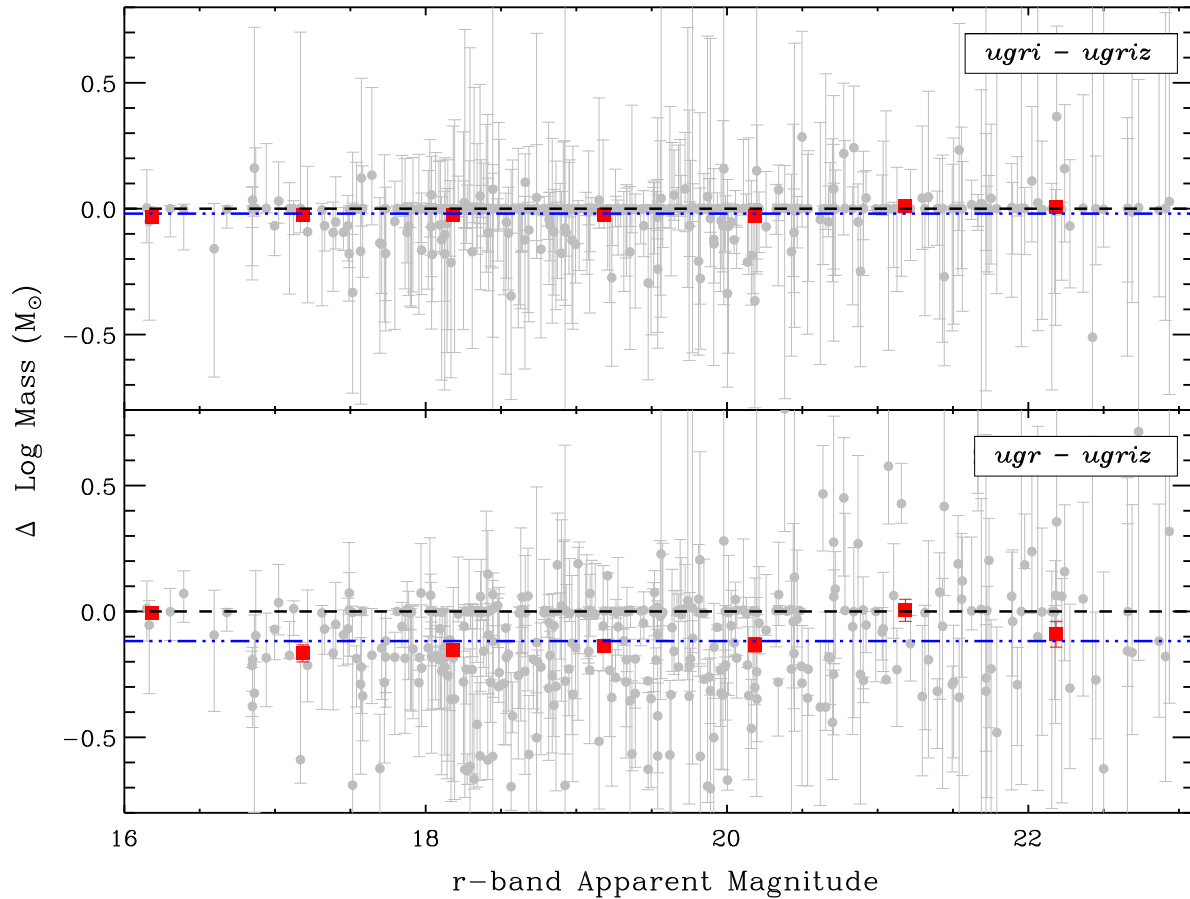


Fig. 12.— *Top*: The stellar mass derived from the PÉGASE.2 SEDs when all five SDSS filters $ugriz$ are used in fit compared to when only $ugri$ are used as a function of apparent magnitude. *Bottom*: Same as above, except only three filters (ugr) are used. Individual galaxies are plotted in grey, with red squares indicating the values determined when the sample has been binned. The black, dashed line indicates no difference, while the blue (dashed-dotted) line indicates the mean difference.

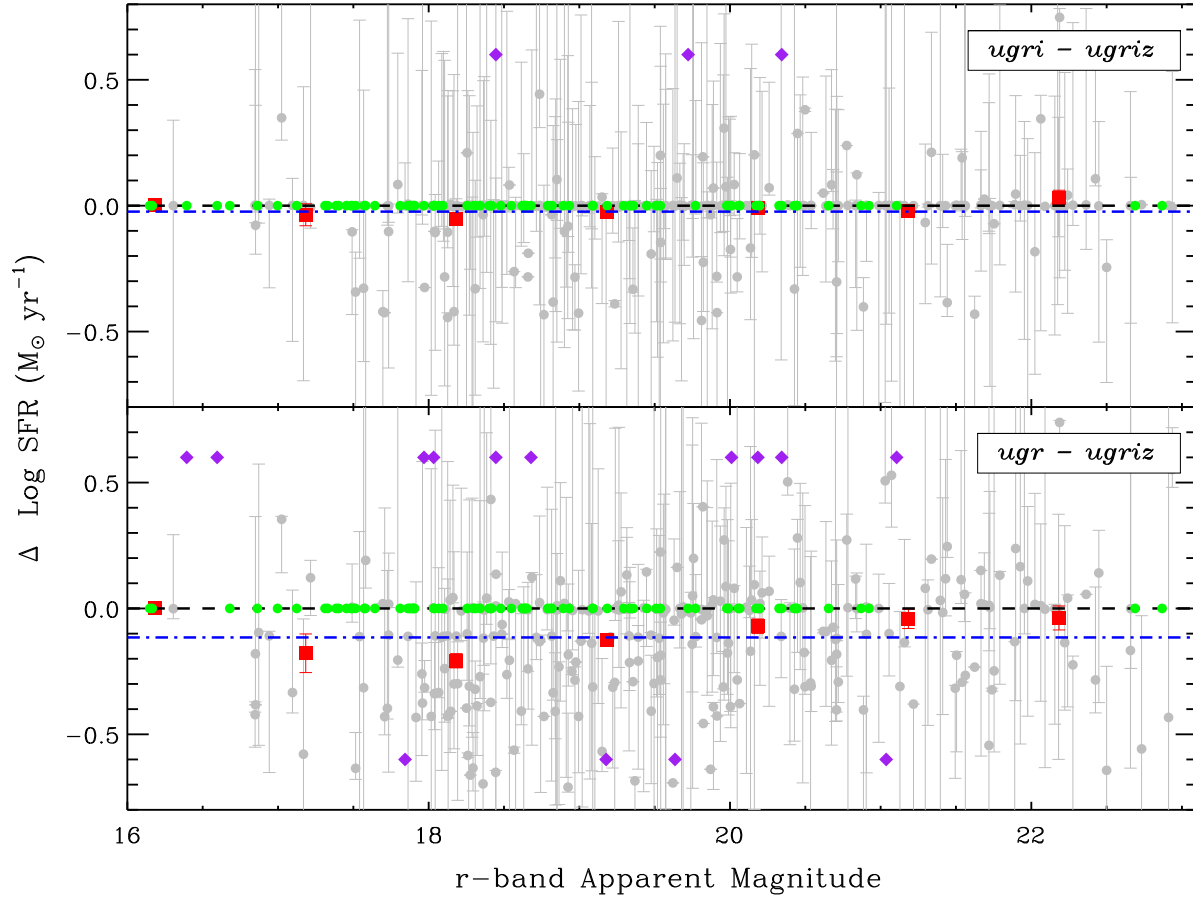


Fig. 13.— *Top*: The star-formation rate derived from the PÉGASE.2 SEDs when all five SDSS filters *ugriz* are used in fit compared to when only *ugri* are used as a function of apparent magnitude. *Bottom*: Same as above, except only three filters (*ugr*) are used. Individual star-forming galaxies are plotted in grey, with red points indicating the values determined when these galaxies have been binned. Green points (plotted at $\Delta \log(\text{SFR}) = 0$) indicate those that are determined to be passive in both cases, while purple diamonds (shown here at ± 0.6) are those which are determined to be star-forming in only one scenario. The black, dashed line indicates no difference, while the blue (dashed-dotted) line indicates the mean difference.

TABLE 9—Continued

designation		host position		redshift	stellar mass [log M_{\odot}]	SFR ^a [log M_{\odot}/yr]	sSFR ^a [yr^{-1}]	SN ^b
SN ID	IAU	$\alpha(J2000)$	$\delta(J2000)$					
19769	N/A	23 ^h 21 ^m 46.399 ^s	-00°58'34.895 ^{''}	0.1849±0.0219	9.91 ^{+0.05} _{-0.01}	-0.21 < -0.12 < -0.11	-10.03	lc
19772	N/A	00 ^h 50 ^m 39.911 ^s	-01°02'31.125 ^{''}	0.1747±0.0005	10.60 ^{+0.02} _{-0.02}	-99.00 < -99.00 < -99.00	-99.00	gal
19775	2007pc	21 ^h 15 ^m 49.475 ^s	+00°39'04.368 ^{''}	0.1379±0.0005	10.52 ^{+0.16} _{-0.02}	-99.00 < -99.00 < -0.04	-99.00	sn
19787	N/A	00 ^h 01 ^m 07.528 ^s	-00°05'52.365 ^{''}	0.1973±0.0010	10.96 ^{+0.18} _{-0.24}	-99.00 < -99.00 < -99.00	-99.00	gal
19821	N/A	23 ^h 47 ^m 07.083 ^s	+01°01'33.631 ^{''}	0.2376±0.0282	10.16 ^{+0.12} _{-0.02}	-99.00 < -99.00 < -0.39	-99.00	lc
19825	N/A	02 ^h 18 ^m 33.095 ^s	+00°52'51.398 ^{''}	0.1471±0.0117	9.89 ^{+0.02} _{-0.24}	-99.00 < -99.00 < -99.00	-99.00	lc
19833	N/A	02 ^h 35 ^m 29.213 ^s	-01°10'43.283 ^{''}	0.2333±0.0005	10.80 ^{+0.40} _{-0.18}	0.66 < 1.11 < 1.41	-9.69	gal
19913	2007qf	22 ^h 15 ^m 02.930 ^s	-00°20'30.228 ^{''}	0.2038±0.0005	9.84 ^{+0.05} _{-0.01}	0.35 < 0.79 < 0.80	-9.05	sn
19968	2007ol	01 ^h 37 ^m 23.783 ^s	-00°18'42.154 ^{''}	0.0560±0.0002	10.43 ^{+0.10} _{-0.11}	-99.00 < -99.00 < 0.20	-99.00	sn
19969	2007pt	02 ^h 07 ^m 38.356 ^s	-00°19'26.498 ^{''}	0.1753±0.0001	10.50 ^{+0.10} _{-0.18}	0.89 < 1.13 < 1.14	-9.38	sn
19990	2007ps	02 ^h 19 ^m 13.444 ^s	-00°23'04.322 ^{''}	0.2460±0.0050	10.30 ^{+0.07} _{-0.01}	-99.00 < -99.00 < -99.00	-99.00	sn
19992	2007pb	23 ^h 48 ^m 24.946 ^s	-01°11'06.610 ^{''}	0.2278±0.0005	9.53 ^{+0.04} _{-0.07}	0.67 < 0.98 < 0.99	-8.55	sn
20033	N/A	01 ^h 31 ^m 43.340 ^s	-00°43'55.162 ^{''}	0.2002±0.0234	10.08 ^{+0.22} _{-0.16}	-99.00 < -99.00 < -99.00	-99.00	lc
20039	2007qh	00 ^h 39 ^m 31.054 ^s	+01°01'25.271 ^{''}	0.2477±0.0005	11.19 ^{+0.01} _{-0.19}	0.43 < 0.55 < 0.95	-10.64	sn
20048	2007pq	22 ^h 37 ^m 13.945 ^s	+00°44'10.728 ^{''}	0.1855±0.0005	10.62 ^{+0.01} _{-0.10}	-99.00 < -99.00 < -99.00	-99.00	sn
20064	2007om	23 ^h 54 ^m 20.706 ^s	-00°55'02.099 ^{''}	0.1050±0.0002	11.02 ^{+0.19} _{-0.30}	-99.00 < -99.00 < -99.00	-99.00	sn
20084	2007pd	23 ^h 11 ^m 54.353 ^s	-00°34'44.605 ^{''}	0.1399±0.0005	10.60 ^{+0.15} _{-0.22}	0.97 < 1.35 < 1.44	-9.24	sn
20088	N/A	00 ^h 52 ^m 49.281 ^s	+00°37'53.469 ^{''}	0.2444±0.0005	11.02 ^{+0.02} _{-0.05}	0.36 < 0.38 < 0.71	-10.64	sn
20090	N/A	20 ^h 07 ^m 35.999 ^s	-00°04'23.971 ^{''}	0.1987±0.0198	9.85 ^{+1.05} _{-1.03}	0.17 < 1.29 < 1.50	-8.56	lc
20097	2007rd	20 ^h 47 ^m 01.194 ^s	-00°05'55.895 ^{''}	0.2210±0.0050	9.27 ^{+0.31} _{-0.06}	-0.05 < 0.07 < 0.39	-9.20	sn
20111	2007pw	23 ^h 37 ^m 34.578 ^s	+00°14'50.748 ^{''}	0.2450±0.0050	10.57 ^{+0.07} _{-0.01}	-99.00 < -99.00 < -99.00	-99.00	sn
20171	N/A	No Host Detected		0.2399±0.0005	N/A	N/A	N/A	gal
20232	N/A	00 ^h 28 ^m 20.009 ^s	-00°03'29.035 ^{''}	0.2172±0.0005	10.94 ^{+0.23} _{-0.17}	-99.00 < -99.00 < -99.00	-99.00	gal
20350	2007ph	No Host Detected		0.1295±0.0002	N/A	N/A	N/A	sn
20364	2007qo	01 ^h 43 ^m 01.575 ^s	-00°56'42.652 ^{''}	0.2181±0.0009	10.22 ^{+0.29} _{-0.23}	-0.41 < 0.19 < 0.65	-10.03	sn
20376	2007re	21 ^h 17 ^m 34.922 ^s	-00°31'26.276 ^{''}	0.2109±0.0005	10.39 ^{+0.07} _{-0.01}	-99.00 < -99.00 < -99.00	-99.00	sn
20491	N/A	No Host Detected		0.2279±0.0224	N/A	N/A	N/A	lc
20625	2007px	00 ^h 22 ^m 43.951 ^s	-00°28'45.766 ^{''}	0.1082±0.0002	10.55 ^{+0.01} _{-0.07}	0.29 < 0.68 < 0.69	-9.87	sn
20718	2007rj	01 ^h 53 ^m 58.769 ^s	-00°05'36.682 ^{''}	0.0888±0.0001	10.68 ^{+0.05} _{-0.01}	0.10 < 0.11 < 0.70	-10.57	sn
20721	N/A	21 ^h 32 ^m 44.348 ^s	-00°37'21.799 ^{''}	0.2118±0.0001	10.43 ^{+0.07} _{-0.14}	0.87 < 1.18 < 1.20	-9.24	gal
20744	N/A	23 ^h 06 ^m 11.836 ^s	+00°21'32.093 ^{''}	0.2290±0.0233	10.60 ^{+0.01} _{-0.01}	-99.00 < -99.00 < -99.00	-99.00	lc
20768	2007qq	02 ^h 42 ^m 30.377 ^s	-00°58'16.563 ^{''}	0.2376±0.0006	10.37 ^{+0.33} _{-0.09}	-99.00 < -99.00 < -0.24	-99.00	sn
20821	2007rk	03 ^h 42 ^m 17.372 ^s	+01°03'44.187 ^{''}	0.1959±0.0005	10.37 ^{+0.27} _{-0.01}	0.12 < 0.21 < 0.46	-10.16	sn
21033	2007qy	No Host Detected		0.2290±0.0050	N/A	N/A	N/A	sn

^aPassive galaxies are represented by -99.00

^bRedshift used in host galaxy template fitting based on SN spectra (sp), galaxy spectra (gal) or light-curve (lc)

REFERENCES

- Abazajian, K. N., et al. 2009, *ApJS*, 182, 543
- Adelman-McCarthy, J. K., et al. 2006, *ApJS*, 162, 38
- Aldering, G., et al. 2006, *ApJ*, 650, 510
- Astier, P., et al. 2006, *A&A*, 447, 31
- Baldry, I. K., et al., 2006, *MNRAS*, 373, 469
- Blanton, M. R., & Roweis, S. 2007, *AJ*, 133, 734
- Bolzonella, M., Miralles, J.-M., & Pelló, R. 2000, *A&A*, 363, 476
- Branch, D., Livio, M., Yungelson, L. R., Boffi, F. R., & Baron, E. 1995, *PASP*, 107, 1019
- Brinchmann, J., et al. 2004, *MNRAS*, 351, 1151
- Brinchmann, J., & Ellis, R. S. 2000, *ApJ*, 536, L77
- Calzetti, D. 1998, *ArXiv Astrophysics e-prints*
- Cappellaro, E., Evans, R., & Turatto, M. 1999, *A&A*, 351, 459
- Cardelli, J. A., Clayton, G. C., & Mathis, J. S. 1989, *ApJ*, 345, 245
- Chakravarti, I. M., Laha, R. G., & Roy, J. 1967, *Handbook of Methods of Applied Statistics*, Vol. I (USE: John Wiley and Sons)
- D'Agostini, G. 1995, *Nuclear Instruments and Methods in Physics Research A*, 362, 487
- Dahlen, T., et al. 2004, *ApJ*, 613, 189
- D' Andrea, C., et al., 2011, Submitted to *ApJ*
- Dilday, B., et al. 2008, *ApJ*, 682, 262
- Dilday, B., et al. 2010, *ApJ*, 713, 1026
- Donas, J., Deharveng, J. M., Laget, M., Milliard, B. & Huguenin, D. 1987, *A&A*, 180, 12
- Felten, J. E. 1976, *ApJ*, 207, 700
- Fioc, M., & Rocca-Volmerange, B. 1997, *A&A*, 326, 950
- Frieman, J. A., et al. 2008, *AJ*, 135, 338
- Fukugita, et al., 1996, *AJ*, 111, 1748
- Gal-Yam, A., & Maoz, D. 2004, *MNRAS*, 347, 942
- Gallagher, J. S., et al. 2005, *ApJ*, 634, 210
- Giavalisco, M., et al. 2004, *ApJ*, 600, L103
- Glazebrook, K., et al. 2004, *Nature*, 430, 181
- Graur, O., et al. 2011, *arXiv:1102.0005*
- Grazian, A., et al. 2006, *A&A*, 449, 951
- Greggio, L. 2005, *A&A*, 441, 1055
- Gunn, J. E., et al. 1998, *AJ*, 116, 3040
- Gunn, J. E., et al. 2006, *AJ*, 131, 2332
- Gupta, R., et al 2011, Submitted to *ApJ*
- Guy, J., et al. 2007, *A&A*, 466, 11
- Guy, J., et al. 2010, *A&A*, 523, A7
- Guzman, R., et al. 1997, *ApJ*, 489, 559
- Hamuy, M., et al. 1995, *AJ*, 109, 1
- Hamuy, M., et al. 1996, *AJ*, 112, 2391
- Hamuy, M. et al. 2000, *AJ*, 120, 1479
- Höflich, P., et al. 2003, *Stellar Candles for the Extragalactic Distance Scale*, 635, 203
- Holtzman, J. A., et al. 2008, *AJ*, 136, 2306
- Hopkins, A. M., & Beacom, J. F. 2006, *ApJ*, 651, 142
- Howell, D. A., Sullivan, M., Conley, A., & Carlberg, R. 2007, *ApJ*, 667, L37
- Hoyle, F., & Fowler, W. A. 1960, *ApJ*, 132, 565
- Jha, S., Riess, A. G., & Kirshner, R. P. 2007, *ApJ*, 659, 122
- Kasen, D., & Woosley, S. E. 2007, *ApJ*, 656, 661
- Kauffmann, G., et al. 2003, *MNRAS*, 341, 33
- Kelly, P. L., Hicken, M., Burke, D. L., Mandel, K. S., & Kirshner, R. P. 2010, *ApJ*, 715, 743
- Kessler, R., et al. 2009a, *ApJS*, 185, 32
- Kessler, R., et al. 2009b, *PASP*, 121, 1028
- Kessler, R., et al. 2010, *PASP*, 122, 1415

- King, I. R. 1980, ApJ, 241, 474
- Konishi, K., et al. 2011, Submitted to ApJ
- Kroupa, P. 2001, MNRAS, 322, 231
- Lampeitl, H., et al. 2010a, MNRAS, 401, 2331
- Lampeitl, H., et al., 2010b, ApJ, 722, 566
- Le Borgne, D., & Rocca-Volmerange, B. 2002, A&A, 386, 446
- Le Borgne, et al., 2004, A&A, 425, 881
- Li, W., et al., 2011, MNRAS, 412, 1473
- Mannucci, F., Della Valle, M., & Panagia, N. 2006, MNRAS, 370, 773
- Mannucci, F., et al. 2005, A&A, 433, 807
- Maeda, K., et al. 2011, MNRAS, 413, 3075
- Maoz, D., Sharon, K., & Gal-Yam, A. 2010, ApJ, 722, 1879
- Li, W., Filippenko, A. V., Della Valle, M., & Panagia, N. 2011, MNRAS, 412, 1508
- Neill, J. D., et al. 2006, AJ, 132, 1126
- Nobili, S., & Goobar, A. 2008, A&A, 487, 19
- Oemler, Jr., A., & Tinsley, B. M. 1979, AJ, 84, 985
- Oyaizu, H., et al., 2008, ApJ, 674, 768
- Phillips, M. M. 1993, ApJ, 413, L105
- Prieto, J. L., et al. 2007, ArXiv e-prints, 706
- Riess, A. G., et al. 1998, AJ, 116, 1009
- Sako, M., et al. 2008, AJ, 135, 348
- Sako, M., et al. 2011, Accepted for publication in ApJ
- Salim, S., et al. 2005, ApJ, 619, 39
- Sargsyan, L. A., Weedman, D. W., & Houck, J. R. 2010, ApJ, 715, 986
- Scannapieco, E., & Bildsten, L. 2005, ApJ, 629, L85
- Schlegel, D. J., Finkbeiner, D. P., & Davis, M. 1998, ApJ, 500, 525
- Schmidt, M. 1968, ApJ, 151, 393
- Sollerman, J., et al. 2009, ApJ, 703, 1374
- Stephens, M. A. 1974, Journal of the American Statistical Association, 69, 730
- Stoughton, C., et al. 2002, AJ, 123, 485
- Strateva, I., et al. 2001, AJ, 122, 1861
- Strauss, M. A., et al. 2002, AJ, 124, 1810
- Sullivan, M., et al. 2006, ApJ, 648, 868
- Sullivan, M., et al. 2010, MNRAS, 406, 782
- Taylor, E. N., et al. 2009, ApJ, 694, 1171
- Wang, L., Hoefflich, P., & Wheeler, J. C. 1997, ApJ, 483, L29+
- Wood-Vasey, W. M., et al. 2007, ApJ, 666, 694
- York, D. G., et al. 2000, AJ, 120, 1579
- Yungelson, L., & Livio, M. 1998, ApJ, 497, 168
- Zheng, C., et al. 2008, AJ, 135, 1766